

Continuous wave quantum light control via engineered Rydberg induced dephasing

Iason Tsiamis,^{1,2,*} Oleksandr Kyriienko,³ and Anders S. Sørensen⁴

¹*Dahlem Center for Complex Quantum Systems and Fachbereich Physik,
Freie Universität Berlin, 14195 Berlin, Germany*

²*The Niels Bohr Institute, University of Copenhagen,
Blegdamsvej 17, DK-2100 Copenhagen, Denmark*

³*Department of Physics and Astronomy, University of Exeter,
Stocker Road, Exeter EX4 4QL, United Kingdom*

⁴*Center for Hybrid Quantum Networks (Hy-Q), The Niels Bohr Institute,
University of Copenhagen, DK-2100 Copenhagen Ø, Denmark*

We analyze several variations of a single-photon optical switch operating in the continuous wave regime, as presented in the accompanying paper [1]. The devices are based on ensembles of Rydberg atoms that interact through van der Waals interaction. Continuously probing the atomic cloud with a weak coherent probe field, under the conditions of electromagnetically induced transparency (EIT) leads to total reflection/transmission of the probe in the absence of control photons. Exciting a Rydberg state with a single control photon breaks the EIT conditions, drastically altering the probe's reflectance/transmittance. We examine how the collective Rydberg interaction in an atomic ensemble enclosed in an optical cavity or in free space induces two probe-induced dephasing processes. These processes localize the control photons and modify the probe's reflectance/transmittance, enhancing the lifetime of control excitations and increasing the devices' efficiency. The devices are characterized by the probability to absorb a control photon and the associated gain as described by the change in the probe's reflectance/transmittance. The results are confirmed through numerical calculations of realistic one- and three-dimensional atomic ensembles in a cavity and an one-dimensional atomic ensemble in free space. The proposed continuous wave devices complement previously realized single photon transistors and expand the possible quantum light manipulation circuitry.

I. INTRODUCTION

The interaction between atoms and light has been a central research topic since the early days of quantum mechanics. In recent decades, significant progress has been made in realizing a quantum interface between a large number of atoms, known as an atomic ensemble, and quantum light. This has been achieved by effectively coupling a collective superposition state of many atoms to quantum light [2]. The interaction of light with multiatom ensembles has resulted in numerous applications for quantum information processing, including quantum memories [3, 4] and quantum repeaters [5, 6]. These applications take advantage of the collective quantum behavior of the atomic ensemble to store and process quantum information encoded in light, enabling the development of more advanced quantum technologies.

Atomic ensembles with Rydberg excitations have captured significant attention in recent years due to their characteristic non-linear properties arising from their strong van der Waals interaction. Their utilization has contributed to significant progress in quantum optics [7–10], enabling the realization of strong photon-photon interactions [11, 12]. This has led to proposals for numerous applications such as Wigner crystallization [13] and quantum gates [14–18]. The high degree of control and strong interaction also makes Rydberg atoms a promising

platform for quantum simulation [19–24] and quantum optimization [25–27].

The potential of Rydberg atoms as a platform for efficient optical control has been demonstrated by several Rydberg-based coherent switches, offering quantum optical control of light by light [28–31]. The fundamental limit of such a switch is the single photon transistor (SPT), which was first proposed for a surface plasmon coupled to an atom in a waveguide [32]. Similar single photon transistors (SPTs) have been realized in various other systems [33–36]. However, these devices operate in the regime where the control photon and probe are applied separately, preventing continuous wave operation. A continuous wave (CW) SPT was proposed in the microwave regime [37–41], but to our knowledge, there has been no CW SPT proposed in the optical regime.

In this paper, we examine several variations of the CW single photon transistor based on an ensemble of driven Rydberg atoms, presented in the accompanying paper [1]. The two versions we theoretically study place the ensemble in free space or inside a single-sided cavity. For the proposed devices, the absence or presence of a single control photon is distinguished by measuring the probe field. When there is no control photon, the system is in the electromagnetically induced transparency (EIT) regime, which allows the probe field to propagate through the ensemble without loss [2, 42]. When a single control photon enters the system and is converted into a long-lived collective Rydberg excitation, it results in interaction-induced blockade [43] and lifts the EIT condition of the probe field, which leads to a measurable signal.

* iason.tsiamis@fu-berlin.de

To achieve a long storage time and high gain of the transistor, we engineer the probe-induced dephasing of the control photons. This enables CW operation of all driving fields throughout the entire protocol, thereby simplifying the protocol and extending the possible applications of the transistor. Notably, our proposed devices can serve as efficient optical single-photon detectors with large signal-to-noise ratio [37]. We further believe that this study opens new possibilities for the application of Rydberg atoms in quantum information processing and quantum communication.

The remainder of this paper is structured as follows. In section II, the realization of the proposed CW SPT device based on a single-sided cavity is discussed, while in section III, the free-space version of the device is analyzed. Both sections are divided into five subsections. In subsection A the model is introduced, while in subsection B the modification of the scattering properties of the probe field and the dephasing induced on the control branch are examined. In subsection C, the optimal impedance matching conditions for control photon storage are theoretically estimated. In subsection D, the Monte Carlo wave-function method used to simulate the system is presented, and in subsection E, the results of the simulation are used to characterize the efficiency of the proposed devices and are compared with the theoretical estimates. Finally, in section IV, we provide the conclusions of our work.

II. CAVITY

A. Model

We begin by introducing the version of the SPT consisting of a Rydberg atomic cloud placed in a single-sided cavity. The cavity is subject to two driving fields and two weak fields, serving as probe and control field respectively, as illustrated in Fig. 1(a). In Fig. 1(b) we show the relevant energetic structure of the Rydberg atoms, which was previously used for pulsed operation [44]. The Hamiltonian for the system is composed of several parts

$$\hat{\mathcal{H}} = \hat{\mathcal{H}}_{\text{probe}} + \hat{\mathcal{H}}_{\text{control}} + \hat{\mathcal{H}}_{\text{Ryd}} + \hat{\mathcal{H}}_{\text{input}} + \hat{\mathcal{H}}_{\text{res}}. \quad (1)$$

Here, $\hat{\mathcal{H}}_{\text{probe}}$ represents the atomic branch used for probing (left branch in Fig. 1(b)), $\hat{\mathcal{H}}_{\text{control}}$ corresponds to the branch responsible for single-photon storage of the control field (right branch in Fig. 1(b)), and $\hat{\mathcal{H}}_{\text{Ryd}}$ describes the Rydberg interaction between the atoms. Additionally, we have introduced the coupling to a continuum $\hat{\mathcal{H}}_{\text{input}}$, providing input and output for the cavity, and the reservoir Hamiltonian $\hat{\mathcal{H}}_{\text{res}}$.

The probe part of the Hamiltonian is given by

$$\hat{\mathcal{H}}_{\text{probe}} = - \sum_{l=1}^N \hbar(g_p \hat{a}_p \hat{\sigma}_{e_p g}^l + \Omega_p \hat{\sigma}_{r_p e_p}^l + \text{h.c.}), \quad (2)$$

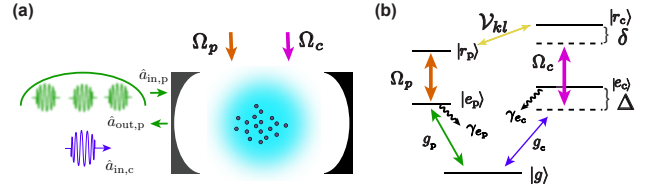


FIG. 1. (a) Sketch of the system, showing the cavity version of the Rydberg-based single photon transistor. An ensemble of Rydberg atoms in the optical cavity is probed by the weak coherent field with intensity $|\alpha_{\text{in},p}|^2$ and driven by nonresonant lasers Ω_c and Ω_p . A control single photon $\hat{a}_{\text{in},c}$ is converted to a Rydberg excitation, which shifts the energy levels, and modifies the reflection of the probe. (b) Atomic level scheme. We consider Rydberg atoms with several states, which can be divided into probe and control Ξ systems (or branches). The left branch ($\{|g\rangle, |e_p\rangle, |r_p\rangle\}$) is responsible for probing by the input field $\alpha_{\text{in},p}$, and operates under EIT conditions in the presence of the drive Ω_p . The right branch ($\{|g\rangle, |e_c\rangle, |r_c\rangle\}$) is responsible for conversion of a single photon from the control pulse to the cavity field, to an $|e_c\rangle$ excitation, and finally to a Rydberg excitation $|r_c\rangle$ exploiting the drive Ω_c .

where the creation (annihilation) operator \hat{a}_p^\dagger (\hat{a}_p) describes a probe cavity photon and g_p is the coupling constant between atoms and probe cavity photons. The energy levels $|e_p\rangle$ and $|r_p\rangle$ are coupled by a classical drive with resonant Rabi frequency of Ω_p . The transition of the l -th atom between states $|m\rangle$ and $|n\rangle$ is described by the operator $\hat{\sigma}_{mn}^l = |m\rangle\langle n|$, where $m, n \in \{g, e_p, r_p, e_c, r_c\}$, and N is the total number of atoms comprising the ensemble. The rotating wave approximation has been performed and the excitation scheme corresponds to EIT conditions, where all fields are resonant with the corresponding transition.

The Hamiltonian that describes the control branch reads

$$\hat{\mathcal{H}}_{\text{control}} = \sum_{l=1}^N \hbar[\Delta \hat{\sigma}_{e_c e_c}^l + \delta \hat{\sigma}_{r_c r_c}^l - (\Omega_c \hat{\sigma}_{r_c e_c}^l + \Omega_c^* \hat{\sigma}_{e_c r_c}^l) + (g_c \hat{a}_c \hat{\sigma}_{e_c g}^l + g_c^* \hat{a}_c^\dagger \hat{\sigma}_{g e_c}^l)], \quad (3)$$

where we have used a rotating frame with respect to the classical drive frequency $\omega_{2,c}$ and the resonance frequency of the cavity $\omega_{1,c}$. The detuning Δ is defined as $\Delta = \omega_{e_c g} - \omega_{1,c}$, while the two photon detuning is $\delta = \Delta - (-\omega_{r_c e_c} + \omega_{2,c})$. Both are depicted in the energy diagram of Fig. 1(b). The atomic transition frequencies are $\omega_{e_c g} = \omega_{e_c} - \omega_g$, $\omega_{r_c e_c} = \omega_{r_c} - \omega_{e_c}$, where the frequencies ω_g , ω_{e_c} , ω_{r_c} correspond to the energies of states $|g\rangle$, $|e_c\rangle$, $|r_c\rangle$, respectively. The operator \hat{a}_c^\dagger describes the control photon, which interacts with each atom with the coupling strength g_c , and the classical drive for the transition between states $|e_c\rangle$ and $|r_c\rangle$ is characterized by the Rabi frequency Ω_c .

The atoms in highly-excited Rydberg states $|r_p\rangle$ and $|r_c\rangle$ interact through the van der Waals interaction, which

is modeled by the interaction Hamiltonian

$$\hat{\mathcal{H}}_{\text{Ryd}} = \hbar \sum_{\substack{l=1 \\ l \neq k}}^N \sum_{k=1}^N \mathcal{V}_{kl} \hat{\sigma}_{r_p r_p}^l \otimes \hat{\sigma}_{r_c r_c}^k, \quad (4)$$

where $\mathcal{V}_{kl} = C_6/\rho_{kl}^6$, with ρ_{kl} denoting the distance between atoms and C_6 is an interaction coefficient [10]. We analyze the system's capability to store control photons and manipulate the probe by distinguishing between the control and probe branches. Our analysis assumes that the control branch receives a single control photon, whereas the probe branch can receive multiple probe photons. The Hamiltonian (4) only considers interaction between atoms excited in the Rydberg states between different branches. This is justified if e.g. the principal quantum number of the control branch is much larger than that of the probe, resulting in a much larger dipole moment. Finally, in order to model the input/output of the system, we add the coupling to the environment and reservoir Hamiltonians, $\hat{\mathcal{H}}_{\text{input}} + \hat{\mathcal{H}}_{\text{res}}$, in the standard form [45, 46].

Using the Hamiltonian (1), we can derive the equations of motion for the operators of the system. Using these equations, we can quantify the storage capability of the control branch and the change in the transmission properties of the probe branch [47, 48]. We assume that the probe branch operates on a much faster timescale than the control branch, indicating a substantial difference in the (EIT/Raman) bandwidths of the two branches. This enables us to examine the probe and control branches separately in the two following subsections.

B. Probing Induced Dephasing

Initially, let us focus on the branch where the continuous probe field is incident (left branch depicted in Fig. 1(b)). In this subsection, we investigate the changes in the scattering properties of the probe field based on the presence or absence of a control photon, which is the primary role of the SPT [32]. Additionally, we examine the effective dephasing mechanisms induced by the continuous probe field on the stored control excitation through the Rydberg interaction.

The dynamics of the probe branch can be fully described by the equations of motion derived from the Hamiltonians $\hat{\mathcal{H}}_{\text{probe}} + \hat{\mathcal{H}}_{\text{Ryd}}$ and the Lindblad jump operators

$$\hat{L}_{\kappa_p} = \sqrt{2\kappa_p} \hat{a}_p, \quad (5)$$

$$\hat{L}_{g_{e_p}}^l = \sqrt{2\gamma_{e_p}} \hat{\sigma}_{g_{e_p}}^l. \quad (6)$$

These operators account for the losses to the environment of the intracavity probe photons and of the l -th atom in the probe excited state $|e_p\rangle$ through spontaneous emission, respectively. We further introduce the decay rate of the cavity probe photons κ_p and the decay

rate of the probe excited state γ_{e_p} . By considering independent Lindblad operators for each atom we implicitly assume that they are coupled to independent reservoirs and hence that emitted photons cannot be absorbed by a different atom.

The Heisenberg equation of motion is used to describe the evolution of system operators through

$$\dot{\hat{o}} = \frac{i}{\hbar} [\hat{\mathcal{H}}, \hat{o}] - \sum_j \left(\hat{L}_j^\dagger \hat{o} \hat{L}_j - \frac{1}{2} \{ \hat{L}_j^\dagger \hat{L}_j, \hat{o} \} \right), \quad (7)$$

where \hat{o} can be any system operator, and \hat{L}_j refers to the system's Lindblad operators. We note that for simplicity we have omitted the Langevin noise operators associated with the decays. This is due to the fact that we consider decay of optical excitation where the reservoir is typically in vacuum. Any such noise operators will always have expectation values corresponding to vacuum noise. Since vacuum noise will never give rise to any excitations of the system, they can be neglected in the following. The resulting equations of motion for the operators associated with the probe branch are found to be

$$\dot{\hat{a}}_p = -\kappa_p \hat{a}_p + \sqrt{2\kappa_p} \hat{a}_{\text{in},p} + i g_p^* \sum_{l=1}^N \hat{\sigma}_{g_{e_p}}^l, \quad (8)$$

$$\dot{\hat{\sigma}}_{g_{e_p}}^l = -\gamma_{e_p} \hat{\sigma}_{g_{e_p}}^l + i g_p \hat{a}_p + i \Omega_p \hat{\sigma}_{g_{r_p}}^l, \quad (9)$$

$$\dot{\hat{\sigma}}_{g_{r_p}}^l = -i \sum_{\substack{k=1 \\ k \neq l}}^N \mathcal{V}_{kl} \hat{\sigma}_{r_c r_c}^k \otimes \hat{\sigma}_{g_{r_p}}^l + i \Omega_p^* \hat{\sigma}_{g_{e_p}}^l. \quad (10)$$

Eq. (8) describes the probe cavity photon's dynamics, accounting for losses to the environment and the input probe field. Eq. (9) captures the evolution of the probe excited state $|e_p\rangle$ of the l -th atom and the interaction with the cavity field and the excitation to the Rydberg state. Eq. (10) tracks the evolution of the l -th atom's Rydberg excitation of the probe branch, which interacts with the Rydberg excitations of the control branch $|r_c\rangle$ of other atoms through van der Waals interactions. We have approximated that the number of atoms is sufficiently large, such that we are operating below the saturation point so that the operators $\hat{\sigma}_{mm}$, where $m \in \{g, e_p, r_p\}$, can be neglected.

The presence of the incident probe field results in the cavity's boundary conditions, described by the input-output relation [50] for the probe cavity photons

$$\hat{a}_{\text{in},p} + \hat{a}_{\text{out},p} = \sqrt{2\kappa_p} \hat{a}_p. \quad (11)$$

The probe input field is considered to be prepared in a coherent state constituted by a strong classical field $\alpha_{\text{in},p}$ and vacuum fluctuations $\delta \hat{a}_{\text{in},p}$ on top of that i.e. $\hat{a}_{\text{in},p} = \alpha_{\text{in},p} + \delta \hat{a}_{\text{in},p}$.

We initially describe the system in the absence of any stored excitation in the control branch, which serves as a reference. By subtracting this reference, we obtain a purely Rydberg-interaction related description.

When there is no stored excitation in the control branch, Eq. (10) simplifies to

$$\dot{\hat{\sigma}}_{gr_p}^l = i\Omega_p^* \hat{\sigma}_{ge_p}^l. \quad (12)$$

Moving to the frequency domain under the Fourier transform

$$\hat{\delta}[\omega] = \int dt e^{i\omega t} \delta[t], \quad (13)$$

where ω is defined with respect to the resonance frequency of the cavity, the solutions of the EOMs (8), (9), and (12) are obtained. The solutions have the form $\hat{\delta} = \bar{\delta} + \mathcal{O}(\delta\hat{a}_{in,p})$ consisting of a strong classical part proportional to the coherent input field $\alpha_{in,p}$ and a part proportional to the quantum fluctuations $\delta\hat{a}_{in,p}$. The average parts of the solutions in the absence of stored control excitation are

$$\bar{a}_p[\omega] = \frac{\sqrt{2\kappa_p} \alpha_{in,p}[\omega]}{\kappa_p - i\omega + \frac{\omega |g_p|^2 N}{\omega(\gamma_{e_p} - i\omega) + i|\Omega_p|^2}}, \quad (14)$$

$$\bar{\sigma}_{ge_p}[\omega] = \frac{g_p \omega \sqrt{2\kappa_p} \alpha_{in,p}[\omega]}{(\kappa_p - i\omega)(\omega(\gamma_{e_p} - i\omega) + i|\Omega_p|^2) + \omega |g_p|^2 N}, \quad (15)$$

$$\bar{\sigma}_{gr_p}[\omega] = \frac{-i\Omega_p g_p \sqrt{2\kappa_p} \alpha_{in,p}[\omega]}{(\kappa_p - i\omega)(\omega(\gamma_{e_p} - i\omega) + i|\Omega_p|^2) + \omega |g_p|^2 N}. \quad (16)$$

Equipped with these solutions, we can evaluate the scattering behavior of the system. The measure of the scattering properties is the reflection coefficient, described by the relation $\hat{a}_{out,p}[\omega] = R_p[\omega] \hat{a}_{in,p}[\omega]$. Using the input-output condition (11) and the solution of the intracavity probe field (14), the reflection coefficient in the absence of a control excitation is found to be

$$R_p[\omega] = \frac{2\kappa_p}{\kappa_p - i\omega + \frac{g_p^2 N \omega}{\omega(\gamma_{e_p} - i\omega) + i|\Omega_p|^2}} - 1. \quad (17)$$

We note that for the probe field being resonant with the cavity i.e. $\omega = 0$, the probe field is fully reflected $R_p[\omega = 0] = 1$. This is due to the device operating under EIT conditions.

Subsequently, we turn to the description of the system in the presence of a stored control excitation. In order to achieve a description of solely the Rydberg-associated processes, the solutions of the probe branch's EOMs in the absence of any stored control excitation (14)-(16) are used as a reference frame. In that spirit, a new set of shifted operators are introduced by subtracting the reference frame from the original operators. The shifted operators of the probe branch are

$$\delta\hat{a}_p[\omega] = \hat{a}_p[\omega] - \bar{a}_p[\omega], \quad (18)$$

$$\delta\hat{\sigma}_{ge_p}^l[\omega] = \hat{\sigma}_{ge_p}^l[\omega] - \bar{\sigma}_{ge_p}[\omega], \quad (19)$$

$$\delta\hat{\sigma}_{gr_p}^l[\omega] = \hat{\sigma}_{gr_p}^l[\omega] - \bar{\sigma}_{gr_p}[\omega], \quad (20)$$

$$\delta\hat{a}_{in,p}[\omega] = \hat{a}_{in,p}[\omega] - \alpha_{in,p}[\omega]. \quad (21)$$

The EOMs of the shifted operators are obtained by substituting the definitions of the shifted operators (18)-(20) into the probe branch's EOMs (8)-(10), which includes the potential presence of a Rydberg excitation on the control branch. The set of EOMs for the shifted probe branch operators in the frequency domain reads

$$-i\omega \delta\hat{a}_p = -\kappa_p \delta\hat{a}_p + \sqrt{2\kappa_p} \delta\hat{a}_{in,p} + ig_p^* \sum_{l=1}^N \delta\hat{\sigma}_{ge_p}^l, \quad (22)$$

$$-i\omega \delta\hat{\sigma}_{ge_p}^l = -\gamma_{e_p} \delta\hat{\sigma}_{ge_p}^l + ig_p \delta\hat{a}_p + i\Omega_p \delta\hat{\sigma}_{gr_p}^l, \quad (23)$$

$$-i\omega \delta\hat{\sigma}_{gr_p}^l = -i \sum_{\substack{k=1 \\ k \neq l}}^N \mathcal{V}_{kl} \hat{\sigma}_{r_c r_c}^k \otimes \delta\hat{\sigma}_{gr_p}^l + i\Omega_p^* \delta\hat{\sigma}_{ge_p}^l + \frac{i\sqrt{2\kappa_p} g_p \alpha_{in,p}}{\Omega_p(\kappa_p - i\omega)} \sum_{\substack{k=1 \\ k \neq l}}^N \mathcal{V}_{kl} \hat{\sigma}_{r_c r_c}^k. \quad (24)$$

As expected a feeding term appears in Eq. (24) in the presence of a stored excitation on the control branch, resulting from the Rydberg-Rydberg interaction between excitations in the probe and control branches. This originates from the fact that in the shifted frame the EOMs of the probe branch describe solely the Rydberg-associated processes.

The solutions of these EOMs are of the form $\hat{\delta}[\omega] = \bar{\delta}[\omega] \hat{\sigma}_{r_c r_c} + \mathcal{O}(\delta\hat{a}_{in}[\omega])$, where the first term is a strong classical term proportional to the amplitude of the probe field α_{in} , conditioned on the presence of a stored control excitation. The second term is a weak quantum term proportional to the differential signal $\delta\hat{a}_{in}$. In the shifted frame the initial state of this operator is the vacuum state. Hence, for the normal ordered products that we will need below, we can simply ignore this operator. The solutions for the probe cavity field and the probe excited state transition operator, for a signal resonant with the cavity i.e. $\omega = 0$, are found to be

$$\delta\hat{a}_p[\omega = 0] = - \sum_{k=1}^N \sqrt{\frac{2}{\kappa_p}} \frac{\alpha_{in,p} C_{b,p}^k}{1 + C_{b,p}^k} \hat{\sigma}_{r_c r_c}^k, \quad (25)$$

$$\delta\hat{\sigma}_{ge_p}^l[\omega = 0] = \sum_{k=1}^N \frac{ig_p \sqrt{\frac{2}{\kappa_p}}}{\gamma_{e_p} + \frac{|\Omega_p|^2}{i\mathcal{V}_{kl}}} \frac{\alpha_{in,p}}{1 + C_{b,p}^k} \hat{\sigma}_{r_c r_c}^k. \quad (26)$$

The blockaded cooperativity for the probe branch due to a stored excitation in the control Rydberg state of the k -th atom is here introduced as $C_{b,p}^k = \sum_{\substack{l=1 \\ l \neq k}}^N C_{b1,p}^{k,l}$, being the cooperativity of the atoms included in the Rydberg blockaded sphere around the k -th atom. The single atom blockaded cooperativity of the l -th atom due to the k -th atom being excited in the Rydberg state of the control branch is given by $C_{b1,p}^{k,l} = (|g_p|^2 / \kappa_p) / (\gamma_{e_p} - i|\Omega_p|^2 / \mathcal{V}_{kl})$. For fully blockaded atoms $\mathcal{V}_{kl} \gg |\Omega_p|^2 / \gamma_{e_p}$ this yields the standard expression for cooperativity of the probe

branch $C_p = |g_p|^2 N / (\gamma_{e_p} \kappa_p)$, whereas outside the blockade regime $\mathcal{V}_{kl} \ll |\Omega_p|^2 / \gamma_{e_p}$, the blockaded cooperativity is suppressed.

At this point the main function of the SPT becomes evident: in the presence of a stored control excitation in the Rydberg state of the k -th atom $|r_c^k\rangle$, the scattering properties of the probe are altered from the full reflection observed in Eq. (17). This is confirmed by using the input-output relation (11), the solution for the shifted field (25), and the mapping between the shifted and the initial operators (18). From these expressions the reflection coefficient on resonance is found to be

$$R_p^k[\omega = 0] = \frac{1 - C_{b,p}^k}{1 + C_{b,p}^k}, \quad (27)$$

depending on the atom where the control photon is stored. To gain some intuition about this coefficient, let us examine the reflection coefficient in the absence of the driving field Ω_p , which decouples $|r_p\rangle$ from the rest of the system, effectively reducing the probe branch to a 2-level system. In this case, using the reflection coefficient in Eq. (17) is $R_p[\omega = 0] = (1 - C_p)/(1 + C_p)$. In analogy, Eq. (27) can be interpreted as being due to an effective sphere of two level system centered at the excited k -th atom with a radius equal to the Rydberg blockade radius.

As shown in Eq. (27), in the presence of a stored control excitation the blockaded cooperativity $C_{b,p}^k$ modifies the scattering properties of the system. This modification leads in turn to extraction of information regarding the presence and/or location of the stored control excitation. The extraction of information about the presence/location of the stored excitation in the control branch leads to dephasing processes in the control branch. These processes arise from the two Lindblad operators (5)-(6), that in the shifted frame read

$$\hat{L}_{\kappa_p} = - \sum_{k=1}^N \frac{\alpha_{in,p} C_{b,p}^k}{1 + C_{b,p}^k} \hat{\sigma}_{r_c r_c}^k \equiv \sum_{k=1}^N \sqrt{2\gamma_{\kappa_p}^k} \hat{\sigma}_{r_c r_c}^k, \quad (28)$$

$$\hat{L}_{g_{e_p}}^l = \sum_{\substack{k=1 \\ k \neq l}}^N \frac{i2g_p \sqrt{\frac{\gamma_{e_p}}{\kappa_p}} \alpha_{in,p}}{\gamma_{e_p} + \frac{|\Omega_p|^2}{i\mathcal{V}_{kl}}} \frac{\hat{\sigma}_{r_c r_c}^k}{1 + C_{b,p}^k} \equiv \sum_{\substack{k=1 \\ k \neq l}}^N \sqrt{2\gamma_{g_{e_p}}^{k,l}} \hat{\sigma}_{r_c r_c}^k, \quad (29)$$

representing the dephasing of the stored control excitation from a change in cavity reflection of the probe and the dephasing due to spontaneous emission of the l -th atom from the probe excited state $|e_p\rangle$ respectively. The dephasing rates associated with the two processes are given by the relation $\gamma_i = \sum_{k=1}^N \langle r_c^k | \frac{1}{2} \hat{L}_i^\dagger \hat{L}_i | r_c^k \rangle / \langle r_c^k | r_c^k \rangle$

$$\gamma_{\kappa_p} = \sum_{k=1}^N |\gamma_{\kappa_p}^k|^2 = \sum_{k=1}^N \frac{2|C_{b,p}^k|^2}{|1 + C_{b,p}^k|^2} |\alpha_{in,p}|^2, \quad (30)$$

$$\gamma_{g_{e_p}}^l = \sum_{\substack{k=1 \\ k \neq l}}^N |\gamma_{g_{e_p}}^{k,l}|^2 = \sum_{\substack{k=1 \\ k \neq l}}^N \frac{\text{Re}(C_{b1,p}^{k,l}) |\alpha_{in,p}|^2}{|1 + C_{b,p}^k|^2}. \quad (31)$$

Let us first focus on the dephasing operator $\hat{L}_{g_{e_p}}^l$ due to spontaneous emission of the l -th atom from the probe excited state $|e_p\rangle$. Its dependence on which atom decayed (l), provides information to the environment regarding the position of the collective Rydberg excitation leading to localization of the stored control excitation in the vicinity of l . This is evident by the presence of \mathcal{V}_{kl} in the denominator, which localizes the stored excitation around the decayed atom, since $\gamma_{e_p}^{k,l}$ is non zero only for the atoms k for which the distance ρ_{kl} is shorter than the Rydberg blockade radius.

The second dephasing operator \hat{L}_{κ_p} acts on the stored excitation due a change in cavity reflection. This dephasing process does not reveal any information regarding the location of the stored excitation and unlike $\hat{L}_{g_{e_p}}^l$, does not lead to localization. Instead, it reveals information only about the presence of the stored excitation, via the change of the reflected probe field, which is the mechanism behind the proposed SPT. Although this dephasing process is suppressed for $C_{b,p} \ll 1$ as seen in Eq. (30), for larger values of the blockaded cooperativity it is present and detectable as seen by the change in the reflection coefficient in Eq. (27) compared to the full reflection observed in the absence of any stored excitation.

Both dephasing processes are an intricate part of the functioning of the proposed device. The \hat{L}_{κ_p} is the detectable process that is essential for the efficiency of the proposed device, but the $\hat{L}_{g_{e_p}}^l$ process leads to localization which provides a long lifetime for the stored excitation (see subsection II E). An important aspect of the current work is the balancing of these two processes for the optimization of the functionality of the SPT.

Finally, we introduce the total collective dephasing rate of the control stored Rydberg excitation, due to the Rydberg mediated processes of the probe branch

$$\gamma_r = \frac{\gamma_{\kappa_p} + \sum_{l=1}^N \gamma_{g_{e_p}}^l}{N} = \sum_{k=1}^N \frac{2(|C_{b,p}^k|^2 + \text{Re}(C_{b,p}^k))}{N|1 + C_{b,p}^k|^2} |\alpha_{in,p}|^2. \quad (32)$$

This rate is proportional to the strength of the probing field $|\alpha_{in,p}|^2$. We can thus adjust the probing strength $|\alpha_{in,p}|^2$ to optimize impedance matching conditions for the control photon storage by counterbalancing decay processes on the control branch. This will be discussed in subsection II C.

C. Impedance Matching

A critical step for the functioning of the SPT is the conversion of a control photon, incident to the cavity, to a Rydberg collective excitation with near unity probability. In order to achieve that, we analyze the scattering dynamics on the control branch and derive an analytical estimate for the impedance matching conditions.

The dynamics of the control branch can be fully described by the corresponding equations of motion derived

from $\hat{H}_{control}$ and the Lindblad jump operators

$$\hat{L}_{\kappa_c} = \sqrt{2\kappa_c}\hat{a}_c, \quad (33)$$

$$\hat{L}_{g_{e_c}}^l = \sqrt{2\gamma_{e_c}}\hat{\sigma}_{g_{e_c}}^l, \quad (34)$$

$$\hat{L}_{r_c}^l = \sqrt{2\gamma_r}\hat{\sigma}_{r_c}^l. \quad (35)$$

The first two Lindblad operators account for the losses to the environment of the intracavity control photon via the decay of the cavity and the decay of the l -th atom from the control excited state $|e_c\rangle$ via spontaneous emission, respectively. The third Lindblad operator (35) accounts for the total effective dephasing of the control Rydberg state $|r_c\rangle$ due to the decay dynamics of the probe branch's Lindblad operators (5)-(6) mediated by the Rydberg interaction, as derived in subsection II B.

The EOMs for the system operators associated with the control field are derived using the Heisenberg equation (7) and reads

$$\dot{\hat{a}}_c = -\kappa_c\hat{a}_c + \sqrt{2\kappa_c}\hat{a}_{in,c} + ig_c^* \sum_{l=1}^N \hat{\sigma}_{g_{e_c}}^l, \quad (36)$$

$$\dot{\hat{\sigma}}_{g_{e_c}}^l = -(\gamma_{e_c} + i\Delta)\hat{\sigma}_{g_{e_c}}^l + ig_c\hat{a}_c + i\Omega_c\hat{\sigma}_{gr_c}^l, \quad (37)$$

$$\dot{\hat{\sigma}}_{gr_c}^l = -(\gamma_r + i\delta)\hat{\sigma}_{gr_c}^l + i\Omega_c^*\hat{\sigma}_{g_{e_c}}^l, \quad (38)$$

We again move to the frequency domain under the Fourier transformation (13). Solving the control branch's set of EOMs and using the input-output relation for the control field $\hat{a}_{in,c} + \hat{a}_{out,c} = \sqrt{2\kappa_c}\hat{a}_c$, we obtain the reflection coefficient and the susceptibilities corresponding to transitions from the ground state to the excited state $|e_c\rangle$ and to the Rydberg state $|r_c\rangle$

$$R_c[\omega] = \frac{\kappa_c + i\omega - \frac{|g_c|^2 N}{\gamma_{e_c} + i(\Delta - \omega) + \frac{|\Omega_c|^2}{\gamma_r + i(\delta - \omega)}}}{\kappa_c - i\omega + \frac{|g_c|^2 N}{\gamma_{e_c} + i(\Delta - \omega) + \frac{|\Omega_c|^2}{\gamma_r + i(\delta - \omega)}}}, \quad (39)$$

$$\chi_{e_c}[\omega] = \frac{\frac{ig_c\sqrt{2\kappa_c}}{(\gamma_{e_c} + i(\Delta - \omega) + \frac{|\Omega_c|^2}{\gamma_r + i(\delta - \omega)})}}{\kappa_c - i\omega + \frac{|g_c|^2 N}{\gamma_{e_c} + i(\Delta - \omega) + \frac{|\Omega_c|^2}{\gamma_r + i(\delta - \omega)}}}, \quad (40)$$

$$\chi_{r_c}[\omega] = \frac{\frac{-\Omega_c^* g_c \sqrt{2\kappa_c}}{(\gamma_{e_c} + i(\Delta - \omega) + \frac{|\Omega_c|^2}{\gamma_r + i(\delta - \omega)}) + |\Omega_c|^2}}{\kappa_c - i\omega + \frac{|g_c|^2 N}{\gamma_{e_c} + i(\Delta - \omega) + \frac{|\Omega_c|^2}{\gamma_r + i(\delta - \omega)}}}, \quad (41)$$

respectively. These factors connect the control branch's operators with the control input field through $\hat{a}_{out,c} = R_c\hat{a}_{in,c}$, $\hat{\sigma}_{g_{e_c}} = \chi_{e_c}\hat{a}_{in,c}$, $\hat{\sigma}_{gr_c} = \chi_{r_c}\hat{a}_{in,c}$.

The conservation of probability dictates the balancing of the incoming and outgoing scattering processes of the system. For the control branch this translates to the relation

$$\begin{aligned} \langle (\hat{a}_{in,c})^\dagger \hat{a}_{in,c} \rangle &= \langle (\hat{a}_{out,c})^\dagger \hat{a}_{out,c} \rangle + \sum_l \langle (L_{g_{e_c}}^l)^\dagger L_{g_{e_c}}^l \rangle \\ &+ \sum_l \langle (L_{r_c}^l)^\dagger L_{r_c}^l \rangle. \end{aligned} \quad (42)$$

By the use of the proportionality factors (39)-(41), Eq. (42) can be reexpressed as

$$|R_c[\omega]|^2 + \Gamma_{e_c}[\omega] + \Gamma_{r_c}[\omega] = 1, \quad (43)$$

which explicitly represents the conservation of probability. Here, we have introduced the loss probability through spontaneous emission of the control excited state $|e_c\rangle$ given an incident photon $\Gamma_{e_c}[\omega] = 2N\gamma_{e_c}|\chi_{e_c}[\omega]|^2$, the dephasing probability of the Rydberg control state $|r_c\rangle$ given an incident photon $\Gamma_{r_c}[\omega] = 2\gamma_r N|\chi_{r_c}[\omega]|^2$ and the reflectance of the incoming control field $|R_c[\omega]|^2$.

Impedance matching is achieved when the dephasing probability of the Rydberg control state, derived by Eq. (41) as

$$\Gamma_{r_c} = \frac{4C_c \frac{|\Omega_c|^2 \gamma_r}{\gamma_{e_c}}}{\left| \frac{\gamma_r(1+C_c)\gamma_{e_c} + \Delta \left(\frac{|\Omega_c|^2}{\Delta} - \delta \right)}{\gamma_{e_c}} + i \frac{\Delta \gamma_r + \delta(1+C_c)\gamma_{e_c}}{\gamma_{e_c}} \right|^2}, \quad (44)$$

is close to unity and accordingly the reflectance and the decay rate through the excited state are close zero. In this case an incident control photon always leads to a dephasing quantum jump resulting in a collective Rydberg excitation after the jump. In order to accomplish this the effective processes of the system need to be balanced and some of them suppressed. This is achieved by choosing the dephasing rate to be equal the effective output rate of the cavity

$$\gamma_r = C_c \gamma_{e_c} |\Omega_c|^2 / \Delta^2, \quad (45)$$

where $C_c = |g_c|^2 N / (\kappa_c \gamma_{e_c})$ is the cooperativity of the control branch [56]. Moreover, the detuning is chosen to be large compared to the effective decay rate from the control excited state i.e. $\Delta \gg (C_c + 1)\gamma_{e_c}$. This condition is crucial as it ensures that the effective decay rate of the cavity is proportional to the number of atoms participating in the collective excitation [53]. Consequently, localization will lead to suppression of this form of decay. A last condition is necessary in order to counter the AC Stark shift, that is present due to the control branch's classical field Ω_c . This condition requires the two photon detuning to be equal to the AC Stark shift i.e. $\delta = |\Omega_c|^2 / \Delta$. Under these conditions the dephasing probability of the Rydberg state given an incident photon on resonance is found to be

$$\Gamma_{r_c}[\omega = 0] = \frac{1}{1 + \frac{1}{C_c} + \frac{1}{(2C_c)^2}}, \quad (46)$$

which goes to unity for large values of the cooperativity $C_c \gg 1$, leading to fulfilment of the impedance matching requirement. Accordingly, the reflectance of the control field R_c and spontaneous emission loss probability from the excited given an incident photon Γ_{e_c} , go to zero in

the same limit $C_c \gg 1$, since

$$|R_c[\omega = 0]|^2 = \frac{1}{(2C_c + 1)^2}, \quad (47)$$

$$\Gamma_{e_c}[\omega = 0] = \frac{4C_c}{(2C_c + 1)^2}. \quad (48)$$

Under these conditions the control photon is transferred into a collective Rydberg excitation. This analytical estimate is confirmed numerically in subsection II E.

D. Numerical Simulation

In this section the wavefunction Monte Carlo (wfMC) approach is used to simulate the system of a Rydberg atomic ensemble located in a single-sided cavity. We considered $N=1000$ atoms located inside the cavity and three different atomic distributions were examined. The first distribution was a symmetric ring geometry, where the neighboring atoms were equidistant. The constant neighboring distance leads to a constant blockaded cooperativity $C_{b,p}^k$ for $k \in [1, N]$, which consequently leads to identical dephasing rates γ_r^k , $k \in [1, N]$ for all atoms. The second and third distributions investigated were more realistic versions, where the atoms were positioned following Gaussian distributions in 1 and in 3 dimensions. In these more realistic models the blockade cooperativity depends on the position each atom, and consequently so does the dephasing rate. For all the geometries we assume that the atoms have identical coupling constants.

The full system is described by the control Hamiltonian (3), two decay operators (5)-(6) and two dephasing operators (28)-(29). The two dephasing operators effectively describe the probe branch, which has been adiabatically eliminated as in section II B. The corresponding non-Hermitian Hamiltonian of the effectively described system reads

$$\begin{aligned} \hat{\mathcal{H}}_{\text{NH}} = & \hat{\mathcal{H}}_{\text{control}} - \frac{i}{2} \hat{L}_{\kappa_c}^\dagger \hat{L}_{\kappa_c} - \frac{i}{2} \sum_{l=1}^N (\hat{L}_{g_{e_c}}^l)^\dagger \hat{L}_{g_{e_c}}^l \\ & - \frac{i}{2} \hat{L}_{\kappa_p}^\dagger \hat{L}_{\kappa_p} - \frac{i}{2} \sum_{l=1}^N (\hat{L}_{g_{e_p}}^l)^\dagger \hat{L}_{g_{e_p}}^l \end{aligned} \quad (49)$$

The basis of the Hilbert space associated with the system is given by the $(2N + 1)$ - dimensional vector $\{|g, 1\rangle, |e_c^1\rangle, \dots, |e_c^N\rangle, |r_c^1\rangle, \dots, |r_c^N\rangle\}$, as we allow the presence of only a single control photon. The non-Hermitian Hamiltonian projected on this basis can be written in matrix form as the $(2N + 1) \times (2N + 1)$ matrix

$$\mathbf{H}_{\text{NH}} = \begin{pmatrix} -i\kappa_c & g_c & g_c & \dots & g_c & 0 & \dots & \dots & 0 \\ g_c & \Delta - i\gamma_{e_c} & 0 & \dots & 0 & \Omega_c & \ddots & & \vdots \\ g_c & 0 & \Delta - i\gamma_{e_c} & 0 & \dots & 0 & \Omega_c & \ddots & \vdots \\ \vdots & \vdots & \ddots & \ddots & \ddots & \vdots & \ddots & \ddots & 0 \\ g_c & 0 & \dots & 0 & \Delta - i\gamma_{e_c} & 0 & \dots & 0 & \Omega_c \\ 0 & \Omega_c & 0 & \dots & 0 & \delta - i\gamma_r^1 & 0 & \dots & 0 \\ \vdots & \ddots & \Omega_c & 0 & \dots & 0 & \delta - i\gamma_r^2 & \ddots & \vdots \\ \vdots & & \ddots & \ddots & \ddots & \vdots & \ddots & \ddots & 0 \\ 0 & \dots & \dots & 0 & \Omega_c & 0 & \dots & 0 & \delta - i\gamma_r^N \end{pmatrix}$$

where $\gamma_r^k = |\gamma_{\kappa_c}^k| + \sum_l^N |\gamma_{g_{e_c}}^{k,l}|$ is the effective dephasing rate resulting from decay processes on the probe branch (28)-(29).

In a similar manner the wavefunction describing the system at time t is expanded as

$$|\Psi(t)\rangle = c_g |g, 1\rangle + \sum_{l=1}^N c_{e_c}^l(t) |e_c\rangle_l + \sum_{l=1}^N c_{r_c}^l(t) |r_c\rangle_l. \quad (50)$$

Initially the system is de-excited meaning that $c_g(t_0) = c_{e_c}^l(t_0) = c_{r_c}^l(t_0) = 0$, $l \in [0, N]$. The control excitation is introduced to the system by a long single photon pulse of Gaussian profile that starts entering the system at $t = t_0$. This is described by

$$c_{\text{in}}(t) = \frac{1}{4\pi\sigma} e^{-(t-t_0-t_m)^2/(4\sigma^2)}. \quad (51)$$

The input photon pulse is normalized according to $\int_{t_0}^{t_{\text{max}}} dt |c_{\text{in}}(t)|^2 = 1$. The values used for the simulation are $\sigma = 160/\gamma_{e_p}$, $t_m = 500/\gamma_{e_p}$, $t_0 = 0$ and the total duration of the pulse is $t_{\text{tot}} = 1000/\gamma_{e_p}$.

The system evolves under the non-Hermitian Hamiltonian and in the presence of the input pulse the evolution is given by

$$\frac{d}{dt} |\Psi(t)\rangle = -i\mathbf{H}_{\text{NH}} |\Psi(t)\rangle + \sqrt{2\kappa_c} c_{\text{in}}(t) |g, 1\rangle. \quad (52)$$

The total norm of the system's wavefunction and the input pulse at time t is

$$\begin{aligned} \langle \Psi(t) | \Psi(t) \rangle + \int_t^{t_{\text{max}}} |c_{\text{in}}(t)|^2 &= |c_g(t)|^2 \\ &+ \sum_l^N |c_{e_c}(t)|^2 + \sum_l^N |c_{r_c}(t)|^2 + \int_t^{t_{\text{max}}} |c_{\text{in}}(t)|^2. \end{aligned} \quad (53)$$

The norm's initial value is unity at $t = t_0$ and is reduced under the evolution of the non-Hermitian dynamics, while the input is fed into the dissipative system.

As the first step of the process a quantum jump will occur since an incident photon will either be subject to a decoherence quantum jump or the photon will leave the system corresponding to a decay jump. The time of the jump is decided by the standard stochastic procedure of wfMC: A value between 0 and 1 is randomly chosen and the time of the jump set to the temporal point, when the norm reaches that value.

Once the time of jump t_j is set, a second stochastic process determines the nature of the jump as one of the four jump operators (5),(6),(28) or (29). The non-normalized probabilities of these jumps are calculated as

$$p_{\gamma_{gec}}(t_j) = 2\gamma_{ec} \sum_{k=1}^N |c_{ec}^k(t_j)|^2, \quad (54)$$

$$p_{\kappa_c}(t_j) = |\sqrt{2\kappa_c}c_g(t_j) - c_{in}(t_j)|^2, \quad (55)$$

$$p_{\kappa_p}(t_j) = \sum_{k=1}^N |\gamma_{\kappa_p}^k| |c_{rc}^k(t_j)|^2, \quad (56)$$

$$p_{\gamma_{gep}}(t_j) = \sum_{l=1}^N \sum_{\substack{k=1 \\ k \neq l}}^N |\gamma_{ep}^{k,l}| |c_{rc}^k(t_j)|^2, \quad (57)$$

where the dephasing rates $\gamma_{\kappa_p}^k$, $\gamma_{ep}^{k,l}$ were introduced in Eqs. (28)-(29). Additionally, the normalized probabilities Π_i for $i = \{\gamma_{gec}, \kappa_c, \kappa_p, \gamma_{gep}\}$ are found via a normalization process $\Pi_i = p_i(t_j) / \sum_i p_i(t_j)$. Depending on the nature of the jump the evolution of the system takes different paths:

Decay jumps \hat{L}_{κ_c} , $\hat{L}_{\gamma_{gec}}$.—In the cases of one of these two decay jumps, the control photon is lost into the environment by spontaneous emission of one atom from the excited state $|e_c\rangle$ or via decay of the cavity. This type of decay jump concludes the trajectory and the simulation comes to an end.

Dephasing jump $\hat{L}_{\gamma_{gp}}$.—In the occurrence of a dephasing jump due a change in cavity reflection of the probe, the control input photon is fully absorbed by the atoms and the state of the system becomes

$$|\Psi'(t_j)\rangle = \frac{\hat{L}_{\kappa_p} |\Psi(t_j)\rangle}{\sqrt{p_{\kappa_p}(t_j)}}. \quad (58)$$

Then the process is repeated by solving Eq. (52) without an incident field with the subsequent jump determined by the same procedure.

Dephasing jump $\hat{L}_{\gamma_{gep}}$.—In the case of a dephasing jump due to the spontaneous emission of an excited atom in the probe branch, a third stochastic process is necessary in order to identify which of the N atoms decayed from the probe branch's excited state $|e_p\rangle$. The normalized probability of the l -th atom to decay is

$$\Pi_{\gamma_{gep}}^l(t_j) = \frac{p_{\gamma_{gep}}^l(t_j)}{\sum_{l=1}^N p_{\gamma_{gep}}^l(t_j)}, \quad (59)$$

where $p_{\gamma_{gep}}^l(t_j) = \sum_{\substack{k=1 \\ k \neq l}}^N |\gamma_{ep}^{k,l}| |c_{rc}^k(t_j)|^2$. Once the atom that decayed has been determined, the input photon is fully absorbed by the system and the system is prepared in the state

$$|\Psi'(t_j)\rangle = \frac{\hat{L}_{\gamma_{gep}}^l |\Psi(t_j)\rangle}{\sqrt{p_{\gamma_{gep}}^l(t_j)}}, \quad (60)$$

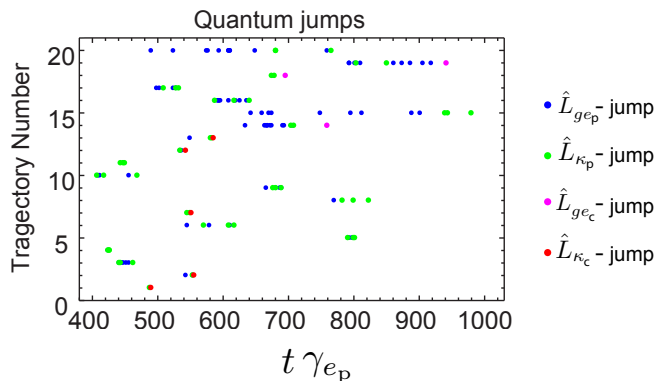


FIG. 2. First 20 trajectories of the Monte Carlo simulation for 3D Gaussian atomic distribution of $N = 1000$ atoms in a cavity with cooperativity $C_c = 100$ and blockaded cooperativity $\bar{C}_{b,p} = 0.5$. The color of the dot indicate the nature of the jump that occur at the specific time. The parameters are fixed to $\Delta/\gamma_{ec} = 180$, $\kappa_p/c = \gamma_{ep/c}$, $\Omega_c/\gamma_{ec} = 5$, $\Omega_p/\gamma_{ec} = 10$, $\delta/\gamma_{ec} = 1.09$, $|\alpha_{in,p}|^2/\gamma_{ec} = 0.33$.

which is localized around the l -th atom that decayed, as explained in the subsection II B. Then the process is repeated for determining the time and the nature of the next jump.

The process is repeated until the control excitation decays through one of the two decay jumps ($\hat{L}_{\gamma_{gec}}$, \hat{L}_{κ_c}) or we determine that sufficiently many \hat{L}_{κ_p} dephasing jumps have occurred that it constitutes a successful switching event.

Our results are averaged over $N_{\text{traj}} = 500$ trajectories for each value of the cooperativity C_c of the control branch and the average blockaded cooperativity $\bar{C}_{b,p} = 1/N \sum_k C_{b,p}^k$ of the probe branch. In Fig. 2 the first 20 trajectories of a simulation with $C_c = 100$ and $\bar{C}_{b,p} = 0.5$ for a 3D atomic Gaussian distribution are depicted. Each trajectory comes to an end, with either successful \hat{L}_{κ_p} dephasing jumps (green dots) or is unsuccessful with one of the decay jumps (pink and red dots). Furthermore it can be observed that the occurrence of $\hat{L}_{\gamma_{gep}}$ dephasing jump is rarely followed by a \hat{L}_{κ_c} decay jump, since the localization induced by the dephasing jump strongly suppresses this type of decay as explained below.

E. Results

The results subsection is organized into three parts. The first focuses on the impedance matching conditions, which are numerically optimized and compared to our analytical estimate derived in the subsection II C. The second part presents the numerical optimization of the efficiency of the SPT versus the cooperativity C_c of the control branch and the average blockaded cooperativity $\bar{C}_{b,p}$ of the probe branch. Finally, in the third part we discuss the effects that limit the efficiency and possible

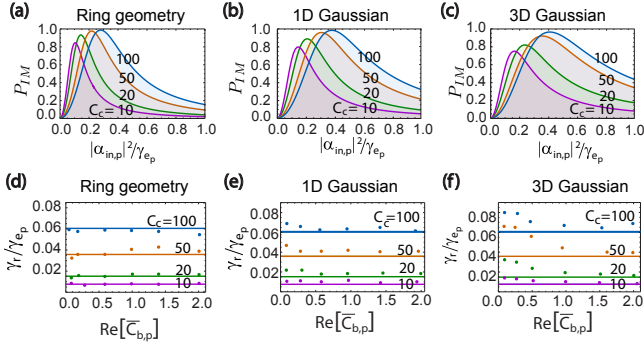


FIG. 3. Impedance matching probability P_{IM} results for the cavity model with $N = 1000$ atoms. (a)-(c) Impedance matching probability as a function of probe strength for $\text{Re}[\bar{C}_{b,p}] = 0.5$ and different values of cooperativity C_c for different atomic distributions: (a) symmetric ring geometry (b) 1D Gaussian (c) 3D Gaussian. (d)-(f) Numerically optimized dephasing rate (dots) and the theoretical estimate (solid line) versus the blocked cooperativity, for $C_c = 10, 20, 50, 100$ and for different atomic distributions: (d) symmetric ring geometry (e) 1D Gaussian (f) 3D Gaussian. The parameters are fixed to $\Delta/\gamma_{e_c} = 180$, $\kappa_{p/c} = \gamma_{e_p/c}$, $\Omega_c/\gamma_{e_c} = 5$, $\Omega_p/\gamma_{e_c} = 10$ and δ varies between $0.14\gamma_{e_c}$ and $0.1\gamma_{e_c}$ to provide better IM.

improvements.

Impedance Matching.—The impedance matching probability P_{IM} is defined as the ratio of the probability of the first jump being a dephasing jump ($\hat{L}_{g_{e_p}}$, \hat{L}_{κ_p}), instead of a decay jump ($\hat{L}_{g_{e_c}}$, \hat{L}_{κ_c}). This is given by the relation

$$P_{\text{IM}} = \frac{\int_{t_0}^{t_{\text{max}}} dt \left(p_{\gamma_{\kappa_p}}(t) + p_{\gamma_{g_{e_p}}}(t) \right)}{\int_{t_0}^{t_{\text{max}}} dt \left(p_{\gamma_{g_{e_c}}}(t) + p_{\kappa_c}(t) + p_{\gamma_{\kappa_p}}(t) + p_{\gamma_{g_{e_p}}}(t) \right)}, \quad (61)$$

where the probabilities for the realization of each jump are defined in Eqs. (54)-(57). It is essential for the function of the SPT that P_{IM} is close to unity, as it sets the upper limit for the efficiency, since it guarantees that the control photon is absorbed by the atomic ensemble.

As shown in Fig. 3 (a)-(c) the optimization is done by varying the strength of the input probe field for different atomic distributions. The parameters can be found in the caption. The simulations are repeated for different values of the control branch's cooperativity $C_c = 10, 20, 40, 100$ and blocked cooperativity $\text{Re}[\bar{C}_{b,p}] \approx 0.25, 0.5, 1, 1.5, 2$ for the symmetric ring geometry, the 1D Gaussian and the 3D Gaussian atomic distribution.

The value of P_{IM} is observed to be very close to the analytically estimated value of Eq. (46). The maximal value for the probability P_{IM} is obtained for $C_c = 100$ and is 0.987 for the symmetric ring geometry, 0.984 for the 1D Gaussian distribution and 0.963 for the 3D Gaussian distribution. The results of the symmetric ring geometry are closer to the theoretical estimate of 0.99, while as the distribution becomes more realistic a small deviation is observed due to deviations from the symmetric model assumed in the analytical estimate.

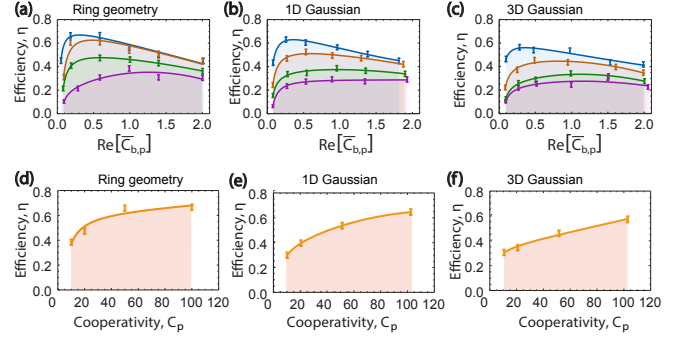


FIG. 4. Efficiency of the cavity model with $N = 1000$ atoms. (a)-(c) Efficiency of the SPT device as a function of blocked cooperativity for control branch cooperativities $C_c = 10, 20, 50, 100$ with the lower curves corresponding to the lower cooperativity. Solid curves show fitted polynomials and serve as a guide to the eye. Results are shown for different atomic distributions: (a) symmetric ring geometry (b) 1D Gaussian (c) 3D Gaussian. (d)-(f) SPT efficiency as a function of cooperativity. At each point the blocked cooperativity was optimized. Results shown for different atomic distributions: (d) symmetric ring geometry (e) 1D Gaussian (f) 3D Gaussian. The parameters are fixed to $\Delta/\gamma_{e_c} = 180$, $\kappa_{p/c} = \gamma_{e_p/c}$, $\Omega_c/\gamma_{e_c} = 5$, $\Omega_p/\gamma_{e_c} = 10$ and δ varies between $0.14\gamma_{e_c}$ and $0.1\gamma_{e_c}$ to provide better IM and $|\alpha_{\text{in},p}|^2$ was chosen to optimize IM at each point.

Furthermore, in the Fig. 3 (d)-(f) the numerically optimized impedance matching conditions for the dephasing rate $\gamma_r^{\text{opt}} = \sum_k^N (\gamma_{\kappa_p}^k + \sum_l^N \gamma_{e_p}^{k,l})$ (dots) are compared to the theoretical estimate (solid line) in Eq. (45). For the symmetric ring case we observe a very close agreement between the two, while as the system becomes more realistic, we observe a small deviation due to the inhomogeneity of the system. For lower values of $\bar{C}_{b,p}$ the deviation that is observed is due to a broad plateau of almost equal P_{IM} probabilities, where the highest value was chosen.

Efficiency.—The final readout of the device can be obtained by counting photons or with a homo- or heterodyne detection scheme, which measures the difference in the output field due to the Rydberg blockade mechanism of the control photon. Alternatively the SPT can be incorporated into an interferometric setup, which cancels the probe signal on a photo detector in the absence of control photons (note that in this case the output is in a coherent state and can hence be cancelled exactly). Since the reflection operator \hat{L}_{κ_p} shown in Eq. (28) exactly corresponds to the difference between having a control photon or not, a detection on such a detector exactly correspond to a \hat{L}_{κ_p} -jump. For simplicity we thus characterize the performance of the proposed SPT device by the number of \hat{L}_{κ_p} -jumps, noting that similar information can also be extracted using homo- or heterodyne detection. In practise we require the number of useful \hat{L}_{κ_p} -jumps to be larger or equal than a fixed threshold number which we take to be $N_{\gamma_{\kappa_p}}^{\text{th}} = 3$. We then define

the efficiency as the probability for this to happen as the corresponding fraction of trajectories

$$\eta = \frac{N_{\text{traj}}(N\gamma_{\kappa_p}^{th} \geq 3)}{N_{\text{traj}}}. \quad (62)$$

For a homodyne measurement scheme this roughly corresponds to a signal squared, which is six times the vacuum noise if we disregard complications due to the multimode nature of the outgoing field.

The simulations are repeated for different values of the control branch's cooperativity $C_c = 10, 20, 40, 100$ and blockaded cooperativity $\text{Re}[\bar{C}_{b,p}] \approx 0.1, 0.25, 0.5, 1, 1.5, 2$ for the symmetric ring geometry, the 1D Gaussian and the 3D Gaussian atomic distribution. The results are shown in Fig. 4. As seen in the figure, the maximal value for the efficiency is obtained for $C_c = 100$ and $\bar{C}_{b,p} \approx 0.25$ and reaches $\eta = 0.666$ for the symmetric ring geometry, $\eta = 0.63$ for the 1D Gaussian distribution and $\eta = 0.562$ for the 3D Gaussian distribution.

It is observed that higher values of the cooperativity of the control branch result in higher efficiency. As a consequence, further improvement of the device is obtainable by increasing the cooperativity, although higher values of the cooperativity are to this day experimentally challenging. According to current experiments, typical values of C_c are in the range of a few 10s [57, 58], however it is anticipated that future devices will attain higher values.

Limitation of Efficiency.—The efficiency of the device is limited by the deleterious jumps responsible for the unsuccessful trajectories, which are the decay $\hat{L}_{g_{ec}}/\hat{L}_{\kappa_c}$ -jumps related to the loss of the input photon excitation due to the decay of an excited atom and loss through the cavity, respectively. For the considered operating conditions the decay through the cavity \hat{L}_{κ_c} jumps happen at a much faster rate, thus limiting the lifetime of the stored excitation.

On one hand, the localization plays an essential role for the functioning of the SPT, as it enhances the lifetime of the stored excitation by suppressing the \hat{L}_{κ_c} jumps. This is achieved through $\hat{L}_{g_{ep}}^l$ jumps by the following mechanism. The storage dynamics transfer the excitation to a collective superposition of all states in $|e_c\rangle$, which has an enhanced decay rate $C_c\gamma_{ec}$. This leads to the input/output rate γ_{out} being enhanced by a factor of $C_c \propto N$ [56]. When the excitation localizes due to a spontaneous emission jump in the probe branch $\hat{L}_{g_{ep}}^l$, revealing information about the location of the excitation on the control branch $|r_c^k\rangle$, the number of atoms participating in the superposition goes down, leading to a reduced decay rate and a longer lifetime. For high values of C_b , the cavity is fully blocked and we only have \hat{L}_{κ_c} jumps, as shown in Fig. 5 (a). This means that the control excitations are not localised and decay rapidly through \hat{L}_{κ_c} jumps, as shown in Fig. 5 (b).

On the other hand, for low C_b we do have very strong localization and the excitation lives long until it is finally lost by spontaneous emission through $\hat{L}_{g_{ec}}$ jump (Fig. 5

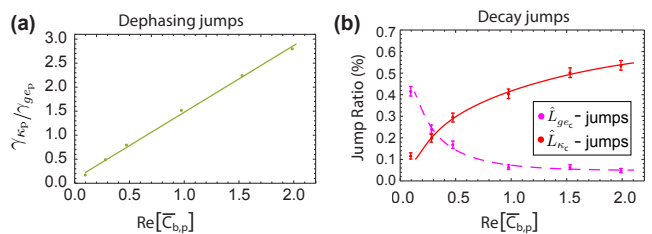


FIG. 5. Dissipative processes for the cavity model of $N = 1000$ atoms with a 3D Gaussian distribution. (a) Ratio of the two dephasing rates versus the blockaded cooperativity for a cooperativity $C_c = 100$. (b) Percentage of unsuccessful trajectories due to spontaneous emission from the probe excited state (magenta dashed line) and decay of the cavity (red solid line) versus the blockaded cooperativity for cooperativity $C_c = 100$. Solid and dashed curves show fitted polynomials and serve as a guide to the eye. The parameters are fixed to $\Delta/\gamma_{ec} = 180$, $\kappa_{p/c} = \gamma_{ep/c}$, $\Omega_c/\gamma_{ec} = 5$, $\Omega_p/\gamma_{ec} = 10$ and δ varies between $0.14\gamma_{ec}$ and $0.1\gamma_{ec}$ to provide better IM and $|\alpha_{\text{in},p}|^2$ was chosen to optimize IM at each point.

(b)). However, a problem arises when C_b is small, despite the prolonged lifetime of the excitation, its impact on the probe's reflection is negligible, making it practically invisible to detection. Since for small C_b the dephasing \hat{L}_{κ_p} jumps are suppressed, as shown in Fig. 5 (a).

As a consequence of the above an optimization process is necessary to optimize, between the processes and the decay rates. The optimal $\bar{C}_{b,p}$ is found at the point where the two sources of decay jumps are equal, as observed when comparing Fig. 4(c) and Fig. 5(b).

Higher value of the cooperativity C_c is beneficial for the functioning of the device, since the localization does not lead to such a dramatic decrease of $\bar{C}_{b,p}$. This results from the fact that the same number of localized atoms will have a higher $\bar{C}_{b,p}$, thus the dephasing \hat{L}_{κ_p} -jumps occur more frequently, while the excitation retains the benefit of an enhanced lifetime due to localization. As a consequence improvement of the efficiency can be achieved by the implementation of a cavity with higher cooperativity C_c , although this may be experimentally challenging. This limitation is not present for the free space model, analyzed in Section III.

III. FREE SPACE

A. System

The second system we consider also consists of a Rydberg atomic cloud, but this time located in free space. As in the cavity case the atomic cloud is subject to two driving fields and two weak fields; one serving as a probe and the other as a control field. The system is sketched in Fig. 6, and assumes propagation of both probe and control signals along the z -axis in the Rydberg medium. N atoms are placed in 1D over a length L . The rele-

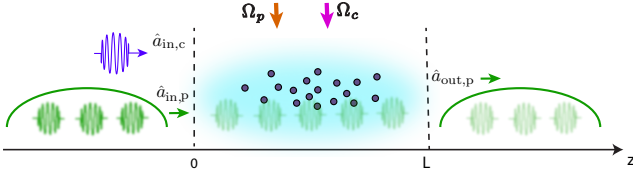


FIG. 6. Sketch of the free space device configuration, where the probe propagates inside the Rydberg cloud which fills part of the system $\{0, L\}$.

vant energy structure of the Rydberg atoms is the same as above and can be seen in Fig. 1(b). The corresponding Hamiltonian consists of several parts, similar to the cavity case,

$$\hat{\mathcal{H}} = \hat{\mathcal{H}}_{\text{probe}} + \hat{\mathcal{H}}_{\text{control}} + \hat{\mathcal{H}}_{\text{Ryd}} + \hat{\mathcal{H}}_{\text{propag}} + \hat{\mathcal{H}}_{\text{res}}, \quad (63)$$

where instead of the $\hat{\mathcal{H}}_{\text{input}}$ describing the input and output for the cavity, we have the propagation of the field through the medium $\hat{\mathcal{H}}_{\text{propag}}$. The probe part reads

$$\begin{aligned} \hat{\mathcal{H}}_{\text{probe}} = & -\hbar \int_0^L dz n(z) (g_p \hat{\mathcal{E}}_p(z, t) \hat{\sigma}_{e_p g}(z, t) \\ & + \Omega_p \hat{\sigma}_{r_p e_p}(z, t) + h.c.), \end{aligned} \quad (64)$$

where a travelling electromagnetic (EM) field on the probing branch at location z is described by the creation (annihilation) operator $\hat{\mathcal{E}}_p^\dagger$ ($\hat{\mathcal{E}}_p$), and couples to the atoms with coupling constant g_p and the classical drive couples the $|e_p\rangle \leftrightarrow |r_p\rangle$ levels with resonant Rabi frequency Ω_p . $n(z)$ is the atomic density of the ensemble. The transition operators $\hat{\sigma}_{mn}(z) = |m\rangle\langle n|$ correspond to the operators for the transition of the atom located at point z between states $|m\rangle$ and $|n\rangle$, $\{m, n\} \in \{g, e_p, r_p, e_c, r_c\}$. Here, the rotating wave approximation was performed and the excitation regime corresponds to EIT conditions.

The Hamiltonian for the control branch under the rotating wave approximation reads

$$\begin{aligned} \hat{\mathcal{H}}_{\text{control}} = & \hbar \int_0^L dz n(z) [\Delta \hat{\sigma}_{e_c e_c}(z, t) + \delta \hat{\sigma}_{r_c r_c}(z, t) \\ & - \Omega_c \hat{\sigma}_{r_c e_c}(z, t) - \Omega_c^* \hat{\sigma}_{e_c r_c}(z, t) \\ & + (g_c \hat{\mathcal{E}}_c \hat{\sigma}_{e_c g}(z, t) + g_c^* \hat{\mathcal{E}}_c^\dagger \hat{\sigma}_{g e_c}(z, t))], \end{aligned} \quad (65)$$

with detuning $\Delta = \omega_{e_c g} - \omega_{1,c}$, where $\omega_{1,c}$ corresponds to the single photon wavepacket central frequency and the two-photon detuning is $\delta = \Delta - (-\omega_{r_c e_c} + \omega_{2,c})$ as above. The single control photon is described by the operator $\hat{\mathcal{E}}_c^\dagger$, which couples to each atom with strength g_c , and the classical drive for the upper transition has strength Ω_c .

The van der Waals interaction Hamiltonian for the ensemble can be written

$$\begin{aligned} \hat{\mathcal{H}}_{\text{Ryd}} = & \hbar \int_0^L dz n(z) \int_0^L dz' n(z') \mathcal{V}(z, z') \times \\ & \times (\hat{\sigma}_{r_p r_p}(z, t) \otimes \hat{\sigma}_{r_c r_c}(z', t)), \end{aligned} \quad (66)$$

where $\mathcal{V}(z, z') = C_6/|z - z'|^6$ and C_6 is an interaction coefficient [10]. Similar to the cavity case, we consider a single incident control photon and allow multiple probe photons, but only include interactions between Rydberg atoms in different branches, assuming their principal quantum numbers to be very different, so that they have very different dipole moments. Lastly, we include the propagation $\hat{\mathcal{H}}_{\text{propag}}$ and the reservoir $\hat{\mathcal{H}}_{\text{res}}$ Hamiltonians.

In the following we consider the dynamics of the probe and control branches separately, by assuming that the characteristic time scales for probing are much faster than for storage of the control photon.

B. Probing Induced Dephasing

We now focus on the branch where the continuous probe field is incident (left branch in Fig. 1(b)). In this subsection we study the modification of the scattering properties of the probe field conditioned on the absence or presence of a control photon, which is the main function of the SPT [32]. Furthermore we describe the effective dephasing processes induced by the continuous probe field on the stored control photon via the Rydberg interaction.

The dynamics of the probe branch are described by the equations of motion derived from the Hamiltonians $\hat{\mathcal{H}}_{\text{probe}} + \hat{\mathcal{H}}_{\text{Ryd}}$, the Lindblad jump operator (6) which accounts for the losses to the environment of the l -th atom on the probe excited state $|e_p\rangle$ through spontaneous emission with a decay rate of γ_{e_p} and the Maxwell equation for light propagation in the medium. The equations of motion for the operators associated with the probe branch are found using the Heisenberg equation (7) to be

$$(\partial_t + c\partial_z) \hat{\mathcal{E}}_p(z, t) = ig_p n(z) L \hat{\sigma}_{g e_p}(z, t), \quad (67)$$

$$\begin{aligned} \partial_t \hat{\sigma}_{g e_p}(z, t) = & -\gamma_{e_p} \hat{\sigma}_{g e_p}(z, t) + ig_p^* \hat{\mathcal{E}}_p(z, t) \\ & + i\Omega_p \hat{\sigma}_{g r_p}(z, t), \end{aligned} \quad (68)$$

$$\begin{aligned} \partial_t \hat{\sigma}_{g r_p}(z, t) = & -i \int_0^L dz' n(z') \mathcal{V}(z, z') \hat{\sigma}_{r_c r_c}(z', t) \otimes \hat{\sigma}_{g r_p}(z, t) \\ & + i\Omega_p^* \hat{\sigma}_{g e_p}(z, t). \end{aligned} \quad (69)$$

Moving to a co-moving frame under the transformation $t' = t - z/c$ with c being speed of light in the medium, absorbing a factor $\sqrt{\frac{c}{L\gamma_{e_p}}}$ in the definition of $\hat{\mathcal{E}}_p$ and assuming g_p real without loss of generality, we define the optical depth of a single atom for the probe branch as $d_{p1} = \frac{g_p^2 L}{c\gamma_{e_p}}$. Dropping the primes on the time coordinate, the equations of motion of the operators associated with

the probe branch are then found to be

$$\partial_z \hat{\mathcal{E}}_p(z, t) = i\sqrt{d_{p1}}n(z)\hat{\sigma}_{ge_p}(z, t), \quad (70)$$

$$\begin{aligned} \partial_t \hat{\sigma}_{ge_p}(z, t) &= -\gamma_{e_p} \hat{\sigma}_{ge_p}(z, t) + i\sqrt{d_{p1}}\gamma_{e_p} \hat{\mathcal{E}}_p(z, t) \\ &+ i\Omega_p \hat{\sigma}_{gr_p}(z, t), \end{aligned} \quad (71)$$

$$\begin{aligned} \partial_t \hat{\sigma}_{gr_p}(z, t) &= -i \int_0^L dz' n(z') \mathcal{V}(z, z') \hat{\sigma}_{r_c r_c}(z', t) \otimes \hat{\sigma}_{gr_p}(z, t) \\ &+ i\Omega_p^* \hat{\sigma}_{ge_p}(z, t), \end{aligned} \quad (72)$$

This system of three equations of motions can be reduced to two by formally integrating the probe field equation (70) and substituting it into Eq. (71). This gives

$$\begin{aligned} \partial_t \hat{\sigma}_{ge_p}(z, t) &= -\gamma_{e_p} \hat{\sigma}_{ge_p}(z, t) - d_{p1} \gamma_{e_p} \int_0^z dz' n(z') \hat{\sigma}_{ge_p}(z', t) \\ &+ i\Omega_L \hat{\sigma}_{gr_p}(z, t) + i\sqrt{d_{p1}} \hat{\mathcal{E}}_p(0, t). \end{aligned} \quad (73)$$

We notice that the field is mediating an effective coupling between the atoms through the absorption of the ensemble. The effective Lindblad operator associated with the atomic effective coupling by propagation through the optically dense ensemble is

$$\hat{L}_{1d_p}(z) = \sqrt{2d_{p1}\gamma_{e_p}} \int_0^z dz' n(z') \hat{\sigma}_{ge_p}(z'). \quad (74)$$

By integrating over the entire length of the ensemble, we obtain the Lindblad jump operator describing the loss of a probe photon by transmission through the entire ensemble. This is given by

$$\hat{L}_{d_p} = \int_0^L dz \hat{L}_{1d_p}(z). \quad (75)$$

As above, we consider the probe input field to be prepared in a coherent state, consisting of a strong classical field $\alpha_{in,p}$ and vacuum fluctuations i.e. $\hat{\mathcal{E}}_p(z=0) = \alpha_{in,p} + \delta\hat{\mathcal{E}}_p(z=0)$. Similarly to our approach for the cavity case in subsection II B, we solve the system in the absence of a stored excitation in the control branch, which we use as a reference, the subtraction of which leads to a purely Rydberg-interaction related description. In the case of no stored excitation in the control branch, the EOM of the transition operator to the probe Rydberg state (72) simplifies to

$$\partial_t \hat{\sigma}_{gr_p}(z, t) = i\Omega_p^* \hat{\sigma}_{ge_p}(z, t). \quad (76)$$

Moving to the frequency domain under the Fourier transform (13) where ω is defined with respect to the central frequency of the photon, we can solve the set of EOMs (70), (71), (76). The solutions have the form $\hat{o} = \bar{o} + \mathcal{O}(\delta\hat{\mathcal{E}}_p(z=0))$ and are comprised of an average part proportional to the coherent input field $\alpha_{in,p}$ and a quantum part proportional to the quantum fluctuations

$\delta\hat{\mathcal{E}}_p(z=0)$. The classical parts of the solutions are then

$$\bar{\mathcal{E}}_p(z, \omega) = e^{-\frac{\int_0^z dz' n(z') \gamma_{e_p} d_{p1} (-i\omega)}{(\gamma_{e_p} - i\omega)(-i\omega) + |\Omega_p|^2}} \alpha_{in,p}(\omega), \quad (77)$$

$$\bar{\sigma}_{ge_p}(z, \omega) = \frac{i\sqrt{d_{p1}}\gamma_{e_p}(-i\omega)\alpha_{in,p}(\omega) e^{-\frac{\int_0^z dz' n(z') \gamma_{e_p} d_{p1} (-i\omega)}{(\gamma_{e_p} - i\omega)(-i\omega) + |\Omega_p|^2}}}{(\gamma_{e_p} - i\omega)(-i\omega) + |\Omega_p|^2}, \quad (78)$$

$$\bar{\sigma}_{gr_p}(z, \omega) = \frac{-\sqrt{d_{p1}}\gamma_{e_p}\Omega_p^* \alpha_{in,p}(\omega) e^{-\frac{\int_0^z dz' n(z') \gamma_{e_p} d_{p1} (-i\omega)}{(\gamma_{e_p} - i\omega)(-i\omega) + |\Omega_p|^2}}}{(\gamma_{e_p} - i\omega)(-i\omega) + |\Omega_p|^2}. \quad (79)$$

The measure of the scattering properties of the system is the transmission coefficient, described by the relation $\hat{\mathcal{E}}_p[L, \omega] = T_p[\omega] \hat{\mathcal{E}}_p[0, \omega]$. Using Eq. (77), the transmission coefficient in the absence of control excitation is

$$T_p[\omega] = e^{\frac{i\omega\gamma_{e_p} d_{p1} N}{(\gamma_{e_p} - i\omega)(-i\omega) + |\Omega_p|^2}}. \quad (80)$$

Since the device is operating under EIT conditions in the absence of control excitation, we note that on resonance the probe field is fully transmitted $T_p[\omega=0] = 1$.

Furthermore, to achieve a description solely of the Rydberg-associated processes, the solutions of the probe branch's EOMs in the absence of any stored control excitation (77)-(79) are used as a reference frame and a new set of shifted operators are introduced by subtracting the reference frame from the original operators. The shifted operators related to the probe branch are then introduced as

$$\delta\hat{\mathcal{E}}_p(z, \omega) = \hat{\mathcal{E}}_p(z, \omega) - \bar{\mathcal{E}}_p(z, \omega), \quad (81)$$

$$\delta\hat{\sigma}_{ge_p}(z, \omega) = \hat{\sigma}_{ge_p}(z, \omega) - \bar{\sigma}_{ge_p}(z, \omega), \quad (82)$$

$$\delta\hat{\sigma}_{gr_p}(z, \omega) = \hat{\sigma}_{gr_p}(z, \omega) - \bar{\sigma}_{gr_p}(z, \omega), \quad (83)$$

$$\delta\hat{\mathcal{E}}_p(z=0, \omega) = \hat{\mathcal{E}}_p(z=0, \omega) - \alpha_{in,p}. \quad (84)$$

The EOMs for the shifted operators are derived by substituting the definitions of the shifted operators (81)-(83) into the EOMs of the probe branch (70)-(72), accounting for the possible presence of a control photon excitation in the control branch. The EOMs for the shifted operators, associated with the probe branch, in the frequency domain are

$$\partial_z \delta\hat{\mathcal{E}}_p(z, \omega) = i\sqrt{d_{p1}}n(z)\delta\hat{\sigma}_{ge_p}(z, \omega), \quad (85)$$

$$\begin{aligned} -i\omega\delta\hat{\sigma}_{ge_p}(z, \omega) &= -\gamma_{e_p} \delta\hat{\sigma}_{ge_p}(z, \omega) + i\Omega_p \delta\hat{\sigma}_{gr_p}(z, \omega) \\ &+ i\sqrt{d_{p1}}\gamma_{e_p} \delta\hat{\mathcal{E}}_p(z, \omega), \end{aligned} \quad (86)$$

$$-i\omega\delta\hat{\sigma}_{gr_p}(z, \omega) = +i\Omega_p^* \delta\hat{\sigma}_{ge_p}(z, \omega)$$

$$\begin{aligned} -i \int_0^L dz' n(z') \mathcal{V}(z, z') \hat{\sigma}_{r_c r_c}(z', \omega) \otimes \delta\hat{\sigma}_{gr_p}(z, \omega) \\ + \frac{i\sqrt{d_{p1}}\gamma_{e_p}\Omega_p^* \alpha_{in} \int_0^L dz' n(z') \mathcal{V}(z, z') \hat{\sigma}_{r_c r_c}(z', \omega)}{(-i\omega)(\gamma_{e_p} - i\omega) + |\Omega_p|^2}. \end{aligned} \quad (87)$$

As observed, a classical feeding term appears in Eq. (87) only in the presence of a stored excitation in the control

branch, resulting from the Rydberg-Rydberg interaction between excitations in the probe and control branches.

The solutions of these EOMs are expressed as $\hat{o}[\omega] = \bar{o}[\omega]\hat{\sigma}_{rr} + \mathcal{O}(\delta\hat{\mathcal{E}}_p[0, \omega])$, where the first term represents a strong classical component dependent on the probe field's amplitude $\alpha_{in,p}$, conditioned on the presence of a stored control excitation. The second term corresponds to a weak quantum component proportional to the differential signal $\delta\hat{\mathcal{E}}_p[0, \omega]$. Neglecting the weak second term, in a similar fashion as for the cavity case, the solution for the probe excited state transition operator, for a resonant signal i.e. $\omega = 0$, is found to be

$$\begin{aligned} \delta\hat{\sigma}_{ge_p}(z) = & -\frac{i\alpha_{in,p}}{\sqrt{d_{p1}}} \int_0^L dz' n(z') \hat{\sigma}_{r_c r_c}(z') d_{b1,p}(z, z') \times \\ & \times \left(\int_0^z dz'' n(z'') d_{b1,p}(z'', z') e^{-\int_{z''}^z dz''' n(z''') d_{b1,p}(z''', z')} - 1 \right). \end{aligned} \quad (88)$$

The single atom blockaded optical depth is defined as the optical depth of an atom located at position z due to the control excitation stored in the Rydberg state $|r_c\rangle$ of the atom located at position z'

$$d_{b1,p}(z, z') = \frac{d_{p1}\gamma_{e_p}}{\gamma_{e_p} + \frac{|\Omega_p|^2}{i\mathcal{V}(z, z')}}. \quad (89)$$

Additionally, the blockaded optical depth of the probe branch due to a stored control excitation in Rydberg state $|r_c\rangle$ of the atom at position z' is given by $d_{b,p}(z') = \int_0^L dz d_{b1,p}(z, z')$.

At this stage, the primary function of the SPT becomes evident. When a control excitation is stored at the Rydberg state $|r_c\rangle$ of the atom positioned at point z' , the scattering properties of the probe field deviate from the full transmission described by Eq. (80). This effect is confirmed by the solution for the probe field in the presence of a stored control excitation, where the resonance transmission coefficient is given by

$$T_p[z', \omega = 0] = e^{-d_{b,p}(z')}, \quad (90)$$

where z' represents the location where the control photon is stored.

Eq. (90) can be interpreted as an effective two-level system sphere centered at point z' with a radius equal to the Rydberg blockade radius, residing within the ensemble of three-level atoms. As is evident from Eq. (80) and (90) the presence of stored excitation modifies the scattering properties of the system, by an amount set by the blockaded optical depth $d_{b,p}(z')$. This modification leads in return to information regarding the presence and/or location of the stored control excitation.

This takes us to the second part of the section, relating to how the extraction of information on the presence/location of the stored excitation in the control branch leads to dephasing processes. These processes

arise from the two Lindblad operators (75) and the equivalent of (29). At this point we note that we can move to a discrete description of our system, by dividing the system into pieces representing a collection of atoms around position z . To do so, the following transformations are used $\hat{\sigma}(z_l, t) \rightarrow \hat{\sigma}^l(t)$, $\int_{z_l}^{z_{l'}} dz n(z) \rightarrow \sum_{i=l}^{l'}$. Subsequently the discrete version of Eqs. (29), (75) in the shifted frame using the solution Eq. (88) read

$$\hat{L}_{d_p} = \sqrt{\frac{d_{p1}}{\gamma_{e_p}}} \sum_{l=1}^N \sum_{\substack{k=1 \\ k \neq l}}^N \sqrt{2\gamma_{ge_p}^{k,l}} \hat{\sigma}_{r_c r_c}^k, \quad (91)$$

$$\hat{L}_{ge_p}^l = \sum_{\substack{k=1 \\ k \neq l}}^N \sqrt{2\gamma_{ge_p}^{k,l}} \hat{\sigma}_{r_c r_c}^k, \quad (92)$$

where the dephasing rate of the Rydberg state of atom k due to the decay of atom l is given by

$$\sqrt{\gamma_{ge_p}^{k,l}} = -i \sqrt{\frac{2\gamma_{e_p}}{d_{p1}}} d_{b1,p}^{k,l} \alpha_{in,p} D_{b,p}^{k,l}, \quad (93)$$

and $D_{b,p}^{k,l} = \sum_{l'=1}^l d_{b1,p}^{k,l'} e^{-\sum_{l''=l'}^{l'} d_{b1,p}^{k,l''}} - 1$ is the blockaded optical depth attenuation due to propagation of the probe in the atomic medium past the l -th atom due to the Rydberg excitation of k -th atom.

These operators represent the dephasing of control excitations due a change in the transmission and the dephasing due to spontaneous emission from the probe excited state $|e_p\rangle$ of the l -th atom respectively. The dephasing rates associated with the two processes are given by $\gamma_i = \sum_{k=1}^N \langle r_c^k | \frac{1}{2} \hat{L}_i^\dagger \hat{L}_i | r_c^k \rangle / \langle r_c^k | r_c^k \rangle$ and read

$$\gamma_{d_p} = \sum_{\substack{k=1 \\ k \neq l}}^N \frac{d_{p1}}{\gamma_{e_p}} \left| \sum_{l=1}^N \sqrt{\gamma_{ge_p}^{k,l}} \right|^2 = \sum_{\substack{k=1 \\ k \neq l}}^N \left| \sum_{l=1}^N d_{b1,p}^{k,l} D_{b,p}^{k,l} \right|^2 |\alpha_{in,p}|^2, \quad (94)$$

$$\gamma_{ge_p}^l = \sum_{\substack{k=1 \\ k \neq l}}^N \left| \gamma_{e_p}^{k,l} \right|^2 = \sum_{\substack{k=1 \\ k \neq l}}^N \frac{2\gamma_{e_p} |\alpha_{in,p}|^2}{d_{p1}} \left| d_{b1,p}^{k,l} D_{b,p}^{k,l} \right|^2. \quad (95)$$

Let us first consider the dephasing operator $\hat{L}_{ge_p}^l$ due to spontaneous of the l -th atom from the probe excited state $|e_p\rangle$. Similar to the description in subsection II B, this operator depends on the specific atom that has undergone decay, and thus imparts information to the environment regarding the collective Rydberg excitation's spatial position. This results in localization of the stored control excitation around the decayed atom. This localization extends the lifetime of the stored control excitation (see subsection III E).

The second dephasing operator \hat{L}_{d_p} acts on the stored excitation due to a change in transmission. This dephasing process reveals information about the presence of the stored excitation via the change of the transmitted probe

field, which can be detected. It leads to a sizeable change of the transmission, for large values of the blockaded optical depth i.e. $d_{b,p} \gg 1$, as seen in Eq. (94). This is the detectable process that allows the readout of the signal (see subsection III E). Unlike the cavity case, this operator also leads to localization, since the storage occurs in an exponentially decaying mode due to the decreasing probability of an excitation propagating through the ensemble without being dephased.

Lastly, we define the total collective dephasing rate of the control stored Rydberg excitation resulting from the Rydberg-mediated decay processes in the probe branch as

$$\gamma_r = \gamma_{d_p} + \sum_{l=1}^N \gamma_{g_{e_p}}^l. \quad (96)$$

This collective dephasing rate is proportional to the intensity of the probing field $|\alpha_{in,p}|^2$. Consequently, we can optimize the impedance matching conditions for control photon storage by appropriately adjusting the strength of the probing field $|\alpha_{in,p}|^2$, as discussed in the following subsection.

C. Impedance Matching

A crucial aspect of the SPT protocol, as also demonstrated for the case of the cavity, is the efficient conversion of an incident control photon into a Rydberg collective excitation with a high probability. To accomplish this, we examine the scattering dynamics occurring in the control branch and derive an analytical estimate for the optimal impedance matching conditions.

The dynamics of the control branch are described by the EOMs for the corresponding operators derived from $\hat{H}_{control}$, the Maxwell equation for light propagation in the medium and the Lindblad jump operators

$$\hat{L}_{g_{e_c}}(z) = \sqrt{2\gamma_{e_c}} \hat{\sigma}_{g_{e_c}}(z), \quad (97)$$

$$\hat{L}_{r_c}(z) = \sqrt{2\gamma_{r_c}} \hat{\sigma}_{r_c}(z). \quad (98)$$

The first Lindblad operator accounts for the losses to the environment via spontaneous emission from the control excited state $|e_c\rangle$ of the atom located at point z . The second Lindblad operator (98) characterizes for the total effective dephasing of the control Rydberg state $|r_c\rangle$, induced by the decay effects of the probe branch's Lindblad operators (91)-(92) mediated by the Rydberg interaction, derived in subsection III B.

The EOMs for the operators associated with the control branch are derived using the Heisenberg equation (7)

and read

$$(\partial_t + c\partial_z)\hat{\mathcal{E}}_c(z, t) = ig_c n(z)L\hat{\sigma}_{g_{e_c}}(z, t), \quad (99)$$

$$\begin{aligned} \partial_t \hat{\sigma}_{g_{e_c}}(z, t) = & -(\gamma_{e_c} + i\Delta)\hat{\sigma}_{g_{e_c}}(z, t) + ig_c^* \hat{\mathcal{E}}_c(z, t) \\ & + i\Omega_c \hat{\sigma}_{g_{r_c}}(z, t), \end{aligned} \quad (100)$$

$$\partial_t \hat{\sigma}_{g_{r_c}}(z, t) = -(\gamma_r + i\delta)\hat{\sigma}_{g_{r_c}}(z, t) + i\Omega_c^* \hat{\sigma}_{g_{e_c}}(z, t). \quad (101)$$

Moving to a co-moving frame under the transformation $t' = t - z/c$, absorbing a factor $\sqrt{\frac{c}{L\gamma_{e_c}}}$ in the definition of $\hat{\mathcal{E}}_c$ and assuming g_c real without loss of generality, we define the optical depth of a single atom for the control branch as $d_{c1} = \frac{g_c^2 L}{c\gamma_{e_c}}$. Dropping the primes on the time coordinate, the equations of motion of the operators associated with the control branch are then found to be

$$\partial_z \hat{\mathcal{E}}_c(z, t) = i\sqrt{d_{c1}} n(z) \hat{\sigma}_{g_{e_c}}(z, t), \quad (102)$$

$$\begin{aligned} \partial_t \hat{\sigma}_{g_{e_c}}(z, t) = & -(\gamma_{e_c} + i\Delta)\hat{\sigma}_{g_{e_c}}(z, t) \\ & + i\sqrt{d_{c1}} \gamma_{e_c} \hat{\mathcal{E}}_c(z, t) + i\Omega_c \hat{\sigma}_{g_{r_c}}(z, t), \end{aligned} \quad (103)$$

$$\partial_t \hat{\sigma}_{g_{r_c}}(z, t) = -(\gamma_r + i\delta)\hat{\sigma}_{g_{r_c}}(z, t) + i\Omega_c^* \hat{\sigma}_{g_{e_c}}(z, t). \quad (104)$$

Subsequently, we move to the frequency domain under the Fourier transform (13). Solving these EOMs of the control branch, we obtain the transmission coefficient and the susceptibilities corresponding to transitions from the ground state to the excited state $|e_c\rangle$ and to the Rydberg state $|r_c\rangle$

$$T_c[\omega] = \exp \left\{ -\frac{\gamma_{e_c} d_c (\gamma_r + i(\delta - \omega))}{(\gamma_{e_c} + i(\Delta - \omega))(\gamma_r + i(\delta - \omega)) + |\Omega_c|^2} \right\}, \quad (105)$$

$$\chi_{e_c}[\omega] = \frac{i\sqrt{d_{c1}}(\gamma_r + i(\delta - \omega))}{((\gamma_{e_c} + i(\Delta - \omega))(\gamma_r + i(\delta - \omega)) + |\Omega_c|^2)} T_c[\omega], \quad (106)$$

$$\chi_{r_c}[\omega] = \frac{-\sqrt{d_{c1}}\Omega_c^*}{((\gamma_{e_c} + i(\Delta - \omega))(\gamma_r + i(\delta - \omega)) + |\Omega_c|^2)} T_c[\omega], \quad (107)$$

respectively. These proportionality factors relate the control branch's operators with the control input field through $\hat{\mathcal{E}}_c(L) = T_c \hat{\mathcal{E}}_c(0)$, $\int_0^L dz \hat{\sigma}_{g_{e_c}} = \chi_{e_c} \hat{\mathcal{E}}_c(0)$ and $\int_0^L dz \hat{\sigma}_{g_{r_c}} = \chi_{r_c} \hat{\mathcal{E}}_c(0)$.

Conservation of probability dictates the balancing of the incoming and outgoing scattering processes of the system. For the scattering effects of the control branch, this reads

$$\begin{aligned} \langle (\hat{\mathcal{E}}_c(0))^\dagger \hat{\mathcal{E}}_c(0) \rangle = & \langle (\hat{\mathcal{E}}_c(L))^\dagger \hat{\mathcal{E}}_c(L) \rangle + \int_0^L dz \langle \hat{L}_{g_{e_c}}^\dagger(z) \hat{L}_{g_{e_c}}(z) \rangle \\ & + \int_0^L dz \langle \hat{L}_{r_c}^\dagger(z) \hat{L}_{r_c}(z) \rangle. \end{aligned} \quad (108)$$

By the use of the proportionality factors (105)-(107), which are independent of the spatial coordinate z , Eq.

(108) can be expressed as

$$|T_c[\omega]|^2 + \Gamma_{e_c}[\omega] + \Gamma_{r_c}[\omega] = 1, \quad (109)$$

where we have introduced the loss probability via spontaneous emission of the control excited state $|e_c\rangle$ for an incident photon $\Gamma_{e_c}[\omega] = 2\gamma_e|\chi_{e_c}[\omega]|^2$, the dephasing probability of the Rydberg control state $|r_c\rangle$ of an incident photon $\Gamma_{r_c}[\omega] = 2\gamma_r|\chi_{r_c}[\omega]|^2$ and the transmittance of the incoming control field $|T_c[\omega]|^2$. Eq. (109) naturally reflects the expected behavior, as it simply expresses the conservation of probability.

In order to be impedance matched, the dephasing probability of the Rydberg control state Γ_{r_c} should be close to unity and accordingly the transmittance and the decay rate through the excited state should be close to zero. In the same way as for the cavity case, we adjust the probe field strength so that the dephasing rate is equal to the decay rate of a fully delocalized Rydberg state, which represent the maximum speed at which excitations can enter the system,

$$\gamma_r = d_c \gamma_{e_c} \Omega_c^2 / (2\Delta^2), \quad (110)$$

where $d_c = d_{c1}N$ is the total optical depth of the control branch [56]. Furthermore, similar to the cavity case, the detuning is chosen to be large compared to the effective decay rate from the control excited state i.e. $\Delta \gg \sqrt{d_c} \gamma_{e_c}$. Under this condition the effective escape rate at the end of the ensemble is proportional to the number of atoms participating in the collective excitation [54, 55], allowing localization to suppress this type of decay. Finally, in order to account for the AC Stark shift, that is present due to the control branch's driving field Ω_c , the two photon detuning is set to be equal to the AC Stark shift i.e. $\delta = |\Omega_c|^2 / \Delta$.

Under these conditions the transmittance on resonance is found to be

$$|T_c[\omega = 0]|^2 = \exp \left\{ -2 \frac{\gamma_e^2 d_c^3 + \frac{d_c^2}{2} + d_c}{(1 + \frac{d_c}{2})^2} \right\}, \quad (111)$$

which goes to zero for large values of the optical depth i.e. $d_c \gg 1$. Accordingly, the dephasing probability of the Rydberg state Γ_{r_c} goes to unity for large optical depth i.e. $d_c \gg 1$, since

$$\Gamma_{r_c}[\omega = 0] = \frac{\frac{d_c}{2}}{1 + \frac{d_c}{2}} (1 - |T_c[\omega = 0]|^2), \quad (112)$$

resulting in the fulfilment of the impedance matching condition. Furthermore, the spontaneous emission loss probability Γ_{e_c} goes to zero in the limit of large optical depth $d_c \gg 2$, since

$$\Gamma_{e_c}[\omega = 0] = \frac{1}{1 + \frac{d_c}{2}} (1 - |T_c[\omega = 0]|^2). \quad (113)$$

This analytical estimate is confirmed by numerical simulations discussed in subsection III E.

D. Numerical Simulation

In the current section we describe the wavefunction Monte Carlo (wfMC) approach used to simulate the system. The system is sketched in Fig. 6, and assumes propagation of both probe and control signals in the Rydberg medium along the z axis. The atomic medium consists of 1000 atoms randomly placed with a Gaussian distribution in 1D over the length L along the z axis. We keep the total optical depth d_c much less than the total number of atoms to represent a situation with weakly coupled atoms. The random neighboring distance between the atoms due to the Gaussian distribution leads to different values of the single atom blockaded optical depths $d_{b,p}^k$ depending on the location of each atom, we thus describe the system using the average blockaded optical depth, defined as $\bar{d}_{b,p} = \frac{1}{N} \sum_{k=1}^N d_{b,p}^k$.

The system is described by the control Hamiltonian (65), two decay operators (75),(97) and two dephasing operators (91)-(92). The two dephasing operators effectively account for the probe branch, which has been adiabatically eliminated using the results of subsection III B. The non-Hermitian Hamiltonian of the full effectively described system in discrete form reads

$$\begin{aligned} \hat{\mathcal{H}}_{NH} = & \hat{\mathcal{H}}_{\text{control}} - \frac{i}{2} \hat{L}_{\kappa_c}^\dagger \hat{L}_{\kappa_c} - \frac{i}{2} \sum_{l=1}^N (\hat{L}_{ge_c}^l)^\dagger \hat{L}_{ge_c}^l \\ & - \frac{i}{2} \hat{L}_{\kappa_p}^\dagger \hat{L}_{\kappa_p} - \frac{i}{2} \sum_{l=1}^N (\hat{L}_{ge_p}^l)^\dagger \hat{L}_{ge_p}^l \end{aligned} \quad (114)$$

The basis of the Hilbert space associated with the system is given by the $2N$ -dimensional vector $\{|e_c^1\rangle, \dots, |e_c^N\rangle, |r_c^1\rangle, \dots, |r_c^N\rangle\}$. The non-Hermitian Hamiltonian projected onto this basis can be written in matrix form as the $2N \times 2N$ matrix

$$\mathbf{H}_{NH} = \begin{pmatrix} \Delta - i\gamma_{e_c} & 0 & \dots & 0 & \Omega & 0 & \dots & 0 \\ -id_c^1 & \Delta - i\gamma_{e_c} & 0 & \dots & 0 & \Omega & \ddots & \vdots \\ \vdots & \ddots & \ddots & \ddots & \vdots & \ddots & \ddots & 0 \\ -id_c^N & \dots & -id_c^1 & \Delta - i\gamma_{e_c} & 0 & \dots & 0 & \Omega \\ \Omega & 0 & \dots & 0 & \delta - \frac{1}{2}i\gamma_r^1 & 0 & \dots & 0 \\ 0 & \Omega & 0 & \dots & 0 & \delta - \frac{1}{2}i\gamma_r^2 & \ddots & \vdots \\ \vdots & \ddots & \ddots & \ddots & \vdots & \ddots & \ddots & 0 \\ 0 & \dots & 0 & \Omega & 0 & \dots & 0 & \delta - \frac{1}{2}i\gamma_r^N \end{pmatrix}$$

where $\gamma_r^k = \sum_{l \neq k}^N |\gamma_{ge_p}^{k,l}| + \frac{d_p^1}{\gamma_{ep}} \left| \sum_{l \neq k}^N \sqrt{\gamma_{ge_p}^{k,l}} \right|^2$ is the effective dephasing rate resulting from decay processes on the probe branch (91)-(92).

In a similar manner as above, the wavefunction describing the system at time t is

$$|\Psi(t)\rangle = \sum_{l=1}^N c_{e_c}^l(t) |e_c\rangle_l + \sum_{l=1}^N c_{r_c}^l(t) |r_c\rangle_l. \quad (115)$$

The system is not excited initially i.e. $c_{e_c}^l(t_0) = c_{r_c}^l(t_0) = 0$, $l \in [1, N]$. The control excitation is introduced to the

system by a long single photon pulse of Gaussian profile that starts entering the system at $t = t_0$ as described above in Eq. (51).

Subsequently, the system evolves under the non-Hermitian Hamiltonian and in the presence of the input pulse is given by the equation

$$\frac{d}{dt} |\Psi(t)\rangle = -i\mathbf{H}_{\text{NH}} |\Psi(t)\rangle + i\sqrt{d_{c1}}\gamma_{e_c}c_{\text{in}}(t) \sum_{l=1}^N |e_c\rangle_l. \quad (116)$$

The norm of the system's wavefunction and the input pulse at time t is

$$\begin{aligned} \langle \Psi(t) | \Psi(t) \rangle + \int_t^{t_{\text{max}}} dt \langle \Psi_{\text{in}}(t) | \Psi_{\text{in}}(t) \rangle &= \\ &= \sum_l^N |c_{e_c}(t)|^2 + \sum_l^N |c_{r_c}(t)|^2 + \int_t^{t_{\text{max}}} |c_{\text{in}}(t)|^2. \end{aligned} \quad (117)$$

The value of the norm is unity at $t = t_0$ and is gradually reduced under the evolution of the non-Hermitian dynamics, while the input enters the dissipative system.

The process begins with a quantum jump which always occurs since the incident photon will either be subject to a decoherence quantum jump or the photon will leave the system corresponding to a decay jump. The time of the jump is determined by the standard stochastic procedure of wfMC. A value between 0 and 1 is randomly chosen and the time of the jump set to the temporal point, when the norm reaches that value.

Once the time of the first jump t_j is set, the nature of the jump is determined through a second stochastic process. It can be one of the four, described by the jump operators Eq.(75),(97),(91)-(92). The non-normalized probabilities of these jumps are

$$p_{\gamma_{g_{e_c}}}(t_j) = 2\gamma_{e_c} \sum_{k=1}^N |c_{e_c}^k(t_j)|^2, \quad (118)$$

$$p_{d_c}(t_j) = \left| i\sqrt{d_{c1}} \sum_{k=1}^N c_{e_c}^k(t_j) - c_{\text{in}}(t_j) \right|^2, \quad (119)$$

$$p_{d_p}(t_j) = \frac{d_{c1}}{\gamma_{e_p}} \sum_{k=1}^N \left| \sum_{\substack{l=1 \\ l \neq k}}^N \sqrt{\gamma_{g_{e_p}}^{k,l}} \right|^2 |c_{r_c}^k(t_j)|^2, \quad (120)$$

$$p_{\gamma_{g_{e_p}}}(t_j) = \sum_{k=1}^N \sum_{\substack{l=1 \\ l \neq k}}^N |\gamma_{g_{e_p}}^{k,l}| |c_{r_c}^k(t_j)|^2, \quad (121)$$

where the dephasing rate $\gamma_{e_p}^{k,l}$ was introduced in Eq. (93). Furthermore, the normalized probabilities Π_i for $i = \{\gamma_{g_{e_c}}, d_c, d_p, \gamma_{g_{e_p}}\}$ are given by a normalization process as $\Pi_i = p_i(t_j) / \sum_i p_i(t_j)$. Depending on the nature of the jump the evolution of the system is determined. The possible outcomes are categorized as:

Decay jumps $\hat{L}_{d_c}, \hat{L}_{\gamma_{g_{e_c}}}$: If either of the two decay jumps occurs, the incident control photon exits the system through spontaneous emission from the excited state

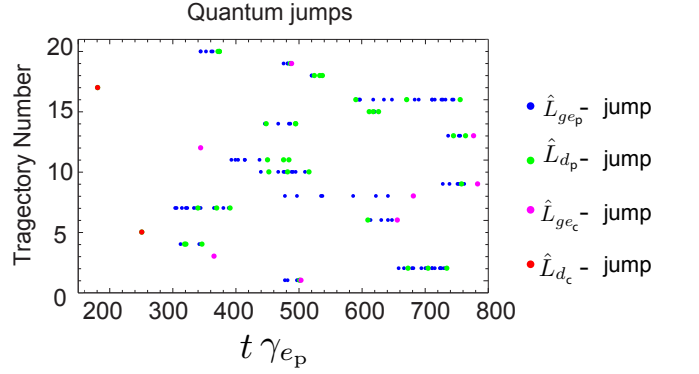


FIG. 7. First 20 trajectories of the Monte Carlo simulation for 1D Gaussian distribution of $N = 1000$ atoms in free space for optical depth $d_c = 100$ and blockaded optical depth $d_{b,p} = 2$. The color of the dots indicates the nature of the jump that occurred at the specific time. The parameters are fixed to $\Delta/\gamma_{e_c} = 40$, $d_p = d_c$, $\gamma_{e_p} = \gamma_{e_c}$, $\Omega_c/\Delta = 0.05$, $\Omega_p/\gamma_{e_c} = 10$, $\delta/\gamma_{e_c} = 0.113$, $|\alpha_{\text{in},p}|^2/\gamma_{e_c} = 0.32$.

or transmission through the atomic ensemble. This type of decay jump marks the end of the trajectory, and the simulation is concluded.

Dephasing jump $\hat{L}_{\gamma_{d_p}}$: In the event of a dephasing jump due a change in transmittance of the probe, the control input photon is absorbed by the system and the state of the system reads

$$|\Psi'(t_j)\rangle = \frac{\hat{L}_{d_p} |\Psi(t_j)\rangle}{\sqrt{p_{\kappa_p}(t_j)}}. \quad (122)$$

Subsequently, the process is repeated in order to determine the time and nature of the following jump. Since the incident input photon pulse was absorbed, we set $c_{\text{in}}(t) = 0$ for $t > t_j$ and the system evolves under the equation $\frac{d}{dt} |\Psi'(t)\rangle = -i\mathbf{H}_{\text{NH}} |\Psi'(t)\rangle$.

Dephasing jump $\hat{L}_{\gamma_{g_{e_p}}}$: When a dephasing jump occurs due to the spontaneous emission of an excited atom in the probe branch, an additional stochastic process becomes essential to determine which specific atom among the ensemble of N atoms decayed from the excited state $|e_p\rangle$ of the probe branch. This process enables the identification of the atom responsible for the effective dephasing. The normalized probability of the l -th atom to decay is given by Eq. (59). After identifying the atom l that decayed, the input photon becomes absorbed by the system, resulting in the preparation of the state described in Eq. (60). This state exhibits localization around the l -th atom that underwent decay, as elucidated in subsection III B. The aforementioned process is then repeated to determine the timing and nature of the subsequent jump.

The process is repeated as many times as necessary until the control excitation undergoes decay via either of the two decay jumps ($\hat{L}_{g_{e_c}}, \hat{L}_{d_c}$), or until three dephasing jumps (\hat{L}_{d_p}) occur, which we again take as the threshold

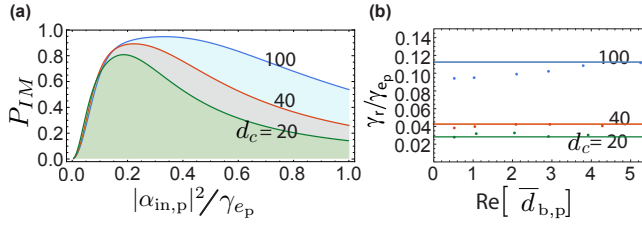


FIG. 8. Impedance matching probability P_{IM} results for the free space model with $N = 1000$ atoms distributed in a Gaussian profile along the z -axis. (a) Impedance matching probability as a function of probe strength for $\text{Re}[\bar{d}_{\text{b,p}}] = 2$ and different values of the total optical depth d_c . (b) Numerically optimized dephasing rate (dots) and the theoretical estimate (solid line) versus the blocked optical depth, for $d_c = 20, 40, 100$. The parameters are fixed to $\Delta/\gamma_{ec} = 40$, $d_p = d_c$, $\gamma_{ep} = \gamma_{ec}$, $\Omega_c/\Delta = 0.05$, $\Omega_p/\gamma_{ec} = 10$, $\delta/\gamma_{ec} = 0.113$.

for a successful trajectory.

The numerical results are averaged over $N_{\text{traj}} = 500$ trajectories for each value of the optical depth d_c of the control branch and the average blocked optical depth $\bar{d}_{\text{b,p}} = 1/N \sum_k^N d_{\text{b,p}}^k$ of the probe branch. The 20 first trajectories of the $d_c = 100$, $\bar{d}_{\text{b,p}} = 2$ simulation for an atomic ensemble with a 1D Gaussian distribution are presented in Fig. 7. It is evident that every trajectory ultimately is concluded either as successful, characterized by three \hat{L}_{d_p} dephasing jumps (green dots), or as unsuccessful, indicated by one of the decay jumps (pink and red dots). Moreover, it is noteworthy that the event of a \hat{L}_{ge_p} dephasing jump due to spontaneous emission of a probe photon is rarely succeeded by a \hat{L}_{d_c} decay jump, denoting the loss of the control photon by transmission through the ensemble. This is due to the fact that the localization effect induced by the dephasing jump strongly suppresses the propagation of the photon.

E. Results

The first part of this subsection focuses on the impedance matching conditions, which are numerically optimized and compared to our analytical estimate derived in subsection III C. The second part of the subsection discusses the numerical optimization of the efficiency of the SPT versus the optical depth d_c of the control branch and the average blocked optical depth $\bar{d}_{\text{b,c}}$ of the probe branch.

Impedance Matching—Similar to above, the impedance matching probability P_{IM} is defined as the ratio of the probability of the first jump being a dephasing jump (\hat{L}_{ge_p} , \hat{L}_{d_p}), instead of a decay jump (\hat{L}_{ge_c} , \hat{L}_{d_c}). This is

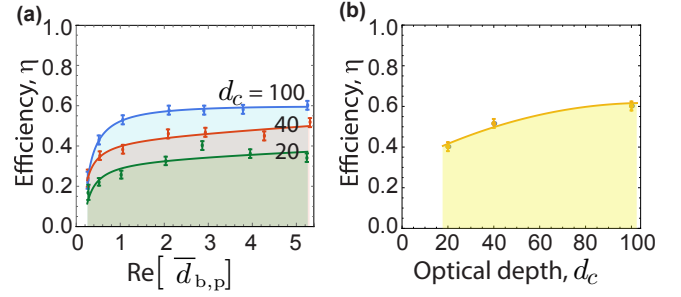


FIG. 9. Efficiency results of the free space model with $N = 1000$ atoms distributed in a Gaussian profile along the z -axis. (a) Efficiency of the SPT device as a function of blocked optical depth for control branch's optical depth $d_c = 20, 40, 100$. Solid curves show fitted polynomials and serve as a guide to the eye. (b) SPT efficiency as a function of cooperativity. At each point the blocked optical depth was fixed to be optimal. The parameters are fixed to $\Delta/\gamma_{ec} = 40$, $d_p/c = \gamma_{ep/c}$, $\Omega_c/\Delta = 0.05$, $\Omega_p/\gamma_{ec} = 10$, $\delta/\gamma_{ec} = 0.113$, and $|\alpha_{\text{in,p}}|^2$ was chosen to optimize IM at each point.

given by the relation

$$P_{\text{IM}} = \frac{\int_{t_0}^{t_{\text{max}}} dt \left(p_{\gamma_{d_p}}(t) + p_{\gamma_{ge_p}}(t) \right)}{\int_{t_0}^{t_{\text{max}}} dt \left(p_{\gamma_{ge_c}}(t) + p_{d_c}(t) + p_{\gamma_{d_p}}(t) + p_{\gamma_{ge_p}}(t) \right)}, \quad (123)$$

where the probabilities for each jump are defined in Eqs. (118)-(121). P_{IM} being close to unity plays a critical role in the operation of the SPT and serves as an upper limit for its efficiency, as it gives the probability the successful absorption of the control photon by the atomic ensemble.

In Fig. 8 (a) we plot the impedance matching probability versus the probe's strength. As seen in the figure, the P_{IM} can be optimized by varying the strength of the incident probe input field's strength. In the optimization the parameters are chosen such that the derived conditions for the detunings are also fulfilled. The simulations are repeated for different values of the control branch's optical depth i.e. $d_c = 20, 40, 100$ and the probe branch's blocked cooperativity i.e. $\text{Re}[\bar{d}_{\text{b,p}}] \approx 0.5, 1, 2, 3, 4, 5$ for the 1D Gaussian atomic distribution.

The value of P_{IM} observed is very close to the theoretically estimated value in Eq. (112). The maximal value $P_{\text{IM}} = 0.947$ is obtained for $d_c = 100$, being close to the theoretical estimate which is $P_{\text{IM}} = 0.98$. We attribute the difference to be due to the non-homogeneous Gaussian distribution.

Moreover, in Fig. 8(b) we plot the numerically optimized impedance matching conditions for the dephasing rate $\gamma_r^{\text{opt}} = \sum_k^N (\gamma_{\kappa_p}^k + \sum_l^N \gamma_{e_p}^{k,l})$ (dots) and the theoretical estimate (solid line) in Eq. (110), versus the blocked optical depth. We find good agreement between the two, with only a slight deviation attributable to the system's inherent inhomogeneity. For lower values of $\bar{d}_{\text{b,p}}$ and $d_c = 100$ the deviation that is observed is due to a long plateau of almost constant P_{IM} , where we have

chosen the highest value.

Efficiency.—As in the cavity case, the efficiency is defined as the number of trajectories in which at least 3 \hat{L}_{d_p} -jumps occur, over the total number of trajectories

$$\eta = \frac{N_{\text{traj}}(N_{\gamma_{d_p}}^{\text{th}} \geq 3)}{N_{\text{traj}}}. \quad (124)$$

In Fig. 9, the results are depicted for different values of the control branch's cooperativity i.e. $d_c = 20, 40, 100$ and the probe branch's blockaded cooperativity i.e. $Re[\bar{d}_{b,p}] \approx 0.5, 1, 2, 3, 4, 5$ for 1D Gaussian atomic distribution. As seen in Fig. 9 the maximal value for the efficiency is obtained for $d_c = 100$ and $\bar{d}_{b,p} \approx 5$ and reaches 0.602. It is observed that higher values of optical depth of the control branch, result in higher efficiency. As a consequence, further improvement can be obtained by increasing the optical depth. Although, although higher values of the optical depth are computationally challenging, they can be achieved experimentally.

IV. CONCLUSIONS

We have conducted a comprehensive analysis and characterization of different variants of an optical single photon transistor capable of operating in the continuous wave regime. These SPT devices are based on ensembles of Rydberg atoms and encompass both free space

and cavity configurations with varying geometries. We analyzed the optimal impedance matching conditions required for efficient capture of single photon, which control the transmission/reflection of the probe field. Additionally, we utilized engineered probe-induced dephasing to optimize the overall efficiency of the devices. The estimated efficiencies can be up to 66%, although we have not performed a full optimisation over all parameters and further improvement might be possible. Furthermore we were limited by the size of our numerical simulations, but we expect the efficiency to rise with the size of the ensemble. The proposed devices may expand the frontiers of CW control in the single photon level, leading to the development of novel tools for optical control and quantum information processing.

ACKNOWLEDGMENTS

This work was supported by the ERC grant QIOS (Grant No. 306576). I.T. acknowledges funding by the Deutsche Forschungsgemeinschaft through the Emmy Noether program (Grant No. ME 4863/1-1). A.S. acknowledges the support of Danmarks Grundforskningsfond (DNRF 139, Hy-Q Center for Hybrid Quantum Networks). O.K. acknowledges the support from EPSRC grants EP/V00171X/1 and EP/X017222/1, and NATO SPS project MYP.G5860.

-
- [1] I. Tsiamis, O. Kyriienko, and A. S. Sørensen, Continuous wave single photon switch based on a Rydberg atom ensemble, submitted to arXiv simultaneously with this article.
 - [2] K. Hammerer, A. S. Sørensen, and E. S. Polzik, Quantum interface between light and atomic ensembles, *Rev. Mod. Phys.* **82**, 1041 (2010).
 - [3] D. Jaksch, J. I. Cirac, P. Zoller, S. L. Rolston, R. Côté, and M. D. Lukin, Fast Quantum Gates for Neutral Atoms, *Phys. Rev. Lett.* **85**, 2208 (2000).
 - [4] M. D. Lukin, M. Fleischhauer, R. Cote, L. M. Duan, D. Jaksch, J. I. Cirac, and P. Zoller, Dipole Blockade and Quantum Information Processing in Mesoscopic Atomic Ensembles, *Phys. Rev. Lett.* **87**, 037901 (2001).
 - [5] A. Kuzmich, W. Bowen, A. Boozer et al., Generation of nonclassical photon pairs for scalable quantum communication with atomic ensembles, *Nature (London)* **423**, 731 (2003).
 - [6] T. Chanelière, D. Matsukevich, S. Jenkins et al., Storage and retrieval of single photons transmitted between remote quantum memories, *Nature (London)* **438**, 833 (2005).
 - [7] A. Browaeys and T. Lahaye, Many-body physics with individually controlled Rydberg atoms, *Nat. Phys.* **16**, 132 (2020).
 - [8] C. S. Adams, J. D. Pritchard, and J. P. Shaffer, Rydberg atom quantum technologies, *J. Phys. B* **53**, 012002 (2020).
 - [9] L. Henriët, L. Beguin, A. Signoles, T. Lahaye, A. Browaeys, G.-O. Reymond, and C. Jurczak, Quantum computing with neutral atoms, *Quantum* **4**, 327 (2020).
 - [10] M. Saffman, T. G. Walker, and K. Mølmer, Quantum information with Rydberg atoms, *Rev. Mod. Phys.* **82**, 2313 (2010).
 - [11] O. Firstenberg, T. Peyronel, Qi-Yu Liang, A. V. Gorshkov, M. D. Lukin, and V. Vuletić, Attractive photons in a quantum nonlinear medium, *Nature (London)* **502**, 71 (2013).
 - [12] A. V. Gorshkov, J. Otterbach, M. Fleischhauer, T. Pohl, and M. D. Lukin, Photon-Photon Interactions via Rydberg Blockade, *Phys. Rev. Lett.* **107**, 133602 (2011).
 - [13] J. Otterbach, M. Moos, D. Muth, and M. Fleischhauer, Wigner Crystallization of Single Photons in Cold Rydberg Ensembles, *Phys. Rev. Lett.* **111**, 113001 (2013).
 - [14] S. Das, A. Grankin, I. Iakoupov, E. Brion, J. Borregaard, R. Boddeda, I. Usmani, A. Ourjoumtsev, P. Grangier, and A. S. Sørensen, Photonic controlled-phase gates through Rydberg blockade in optical cavities, *Phys. Rev. A* **93**, 040303(R) (2016).
 - [15] G. Higgins, F. Pokorny, Chi Zhang, Q. Bodart, and M. Hennrich, Coherent Control of a Single Trapped Rydberg Ion, *Phys. Rev. Lett.* **119**, 220501 (2017).
 - [16] H. Levine, A. Keesling, G. Semeghini, A. Omran, T. T. Wang, S. Ebadi, H. Bernien, M. Greiner, V. Vuletić,

- H. Pichler, and M. D. Lukin, Parallel Implementation of High-Fidelity Multiqubit Gates with Neutral Atoms, *Phys. Rev. Lett.* **123**, 170503 (2019).
- [17] K. McDonnell, L. F. Keary and J. D. Pritchard, Demonstration of a Quantum Gate using Electromagnetically Induced Transparency, *Phys. Rev. Lett.* **129**, 200501 (2022).
- [18] D. Bluvstein, H. Levine, G. Semeghini, T. T. Wang, S. Ebadi, M. Kalinowski, A. Keesling, N. Maskara, H. Pichler, M. Greiner, V. Vuletic, and M. D. Lukin, A quantum processor based on coherent transport of entangled atom arrays, *Nature (London)* **604**, 451 (2022).
- [19] H. Labuhn, D. Barredo, S. Ravets, S. de Leseleuc, T. Macri, T. Lahaye, and A. Browaeys, Tunable two-dimensional arrays of single Rydberg atoms for realizing quantum Ising models, *Nature (London)* **534**, 667 (2016).
- [20] H. Bernien, S. Schwartz, A. Keesling, H. Levine, A. Omran, H. Pichler, S. Choi, A. S. Zibrov, M. Endres, M. Greiner, V. Vuletić, and M. D. Lukin, Probing many-body dynamics on a 51-atom quantum simulator, *Nature (London)* **551**, 579 (2017).
- [21] M. Sbroscia, K. Viebahn, E. Carter, Jr-Chiu Yu, A. Gaunt, and U. Schneider, Observing Localization in a 2D Quasicrystalline Optical Lattice, *Phys. Rev. Lett.* **125**, 200604 (2020).
- [22] S. Ebadi, T. T. Wang, H. Levine, A. Keesling, G. Semeghini, A. Omran, D. Bluvstein, R. Samajdar, H. Pichler, Wen Wei Ho, Soonwon Choi, S. Sachdev, M. Greiner, V. Vuletic, and M. D. Lukin, Quantum phases of matter on a 256-atom programmable quantum simulator, *Nature (London)* **595**, 227 (2021).
- [23] G. Semeghini, H. Levine, A. Keesling, S. Ebadi, T. T. Wang, D. Bluvstein, R. Verresen, H. Pichler, M. Kalinowski, R. Samajdar, A. Omran, S. Sachdev, A. Vishwanath, M. Greiner, V. Vuletic, and M. D. Lukin, Probing Topological Spin Liquids on a Programmable Quantum Simulator, *Science* **374**, 1242 (2021).
- [24] A. J. Daley, I. Bloch, C. Kokail, S. Flannigan, N. Pearson, M. Troyer, and P. Zoller, Practical quantum advantage in quantum simulation, *Nature (London)* **607**, 667 (2022).
- [25] Leo Zhou, Sheng-Tao Wang, Soonwon Choi, H. Pichler, and M. D. Lukin, Quantum Approximate Optimization Algorithm: Performance, Mechanism, and Implementation on Near-Term Devices, *Phys. Rev. X* **10**, 021067 (2020).
- [26] J. R. Weggemans, A. Urech, A. Rausch, R. Spreeuw, R. Boucherie, F. Schreck, K. Schoutens, J. Minar, and F. Spielman, Solving correlation clustering with QAOA and a Rydberg qudit system: a full-stack approach, *Quantum* **6**, 687 (2022).
- [27] S. Ebadi, A. Keesling, M. Cain, T. T. Wang, H. Levine, D. Bluvstein, G. Semeghini, A. Omran, Jinguo Liu, R. Samajdar, Xiu-Zhe Luo, B. Nash, Xun Gao, B. Barak, E. Farhi, S. Sachdev, N. Gemelke, Leo Zhou, Soonwon Choi, H. Pichler, Shengtao Wang, M. Greiner, V. Vuletic, and M. D. Lukin, Quantum Optimization of Maximum Independent Set using Rydberg Atom Arrays, *Science* **376**, 1209 (2022).
- [28] D. Tiarks, S. Baur, K. Schneider, S. Dürr, and G. Rempe, Single-Photon Transistor Using a Förster Resonance, *Phys. Rev. Lett.* **113**, 053602 (2014).
- [29] H. Gorniaczyk, C. Tresp, J. Schmidt, H. Fedder, and S. Hofferberth, Single-Photon Transistor Mediated by Interstate Rydberg Interactions, *Phys. Rev. Lett.* **113**, 053601 (2014).
- [30] S. Baur, D. Tiarks, G. Rempe, and S. Dürr, Single-Photon Switch Based on Rydberg Blockade, *Phys. Rev. Lett.* **112**, 073901 (2014).
- [31] H. Gorniaczyk, C. Tresp, P. Bienias, A. Paris-Mandoki, W. Li, I. Mirgorodskiy, H. P. Büchler, I. Lesanovsky, and S. Hofferberth, Enhancement of Rydberg-mediated single-photon nonlinearities by electrically tuned Förster resonances, *Nat. Commun.* **7**, 12480 (2016).
- [32] D. E. Chang, A. S. Sørensen, E. A. Demler, and M. D. Lukin, A single-photon transistor using nanoscale surface plasmons, *Nat. Phys.* **3**, 807 (2007).
- [33] W. Chen, K. M. Beck, R. Bücker, M. Gullans, M. D. Lukin, H. Tanji-Suzuki, and V. Vuletić, All-Optical Switch and Transistor Gated by One Stored Photon, *Science* **341**, 768 (2013).
- [34] T. G. Tiecke, J. D. Thompson, N. P. de Leon, L. R. Liu, V. Vuletić, and M. D. Lukin, Nanophotonic quantum phase switch with a single atom, *Nature (London)* **508**, 241 (2014).
- [35] Shuo Sun, Hyochul Kim, Zhouchen Luo, G. S. Solomon, and E. Waks, A single-photon switch and transistor enabled by a solid-state quantum memory, *Science* **361**, 57 (2018).
- [36] D. Aghamalyan, Jia-Bin You, Hong-Son Chu, Ching Eng Png, L. Krivitsky, and Leong Chuan Kwek, Tunable quantum switch realized with a single Λ -level atom coupled to the microtoroidal cavity, *Phys. Rev. A* **100**, 053851 (2019).
- [37] O. Kyriienko and A. S. Sørensen, Continuous-Wave Single-Photon Transistor Based on a Superconducting Circuit, *Phys. Rev. Lett.* **117**, 140503 (2016).
- [38] B. Royer, A. L. Grimsmo, A. Choquette-Poitevin, and A. Blais, Itinerant Microwave Photon Detector, *Phys. Rev. Lett.* **120**, 203602 (2018).
- [39] I. Iakoupov, Y. Matsuzaki, W. J. Munro, and S. Saito, Sequential nonabsorbing microwave single-photon detector, *Phys. Rev. Res.* **2**, 033238 (2020).
- [40] A. L. Grimsmo, B. Royer, J. M. Kreikebaum, Yufeng Ye, K. O'Brien, I. Siddiqi, and A. Blais, Quantum Metamaterial for Broadband Detection of Single Microwave Photons, *Phys. Rev. Applied* **15**, 034074 (2021).
- [41] Zhiling Wang, Zenghui Bao, Yan Li, Yukai Wu, Weizhou Cai, Weiting Wang, Xiyue Han, Jiahui Wang, Yipu Song, Luyan Sun, Hongyi Zhang, and Luming Duan, An ultra-high gain single-photon transistor in the microwave regime, *Nat. Commun.* **13**, 6104 (2022).
- [42] M. Fleischhauer, A. Imamoglu, and J. P. Marangos, Electromagnetically induced transparency: Optics in coherent media, *Rev. Mod. Phys.* **77**, 633 (2005).
- [43] E. Urban, T. A. Johnson, T. Henage, L. Isenhower, D. D. Yavuz, T. G. Walker, and M. Saffman, Observation of Rydberg blockade between two atoms, *Nat. Phys.* **5**, 110 (2009).
- [44] Hao, Y.M., Lin, G.W., Lin, X.M. et al. Single-photon transistor based on cavity electromagnetically induced transparency with Rydberg atomic ensemble, *Sci. Rep.* **9**, 4723 (2019).
- [45] A. A. Clerk, M. H. Devoret, S. M. Girvin, F. Marquardt, and R. J. Schoelkopf, Introduction to quantum noise, measurement, and amplification, *Rev. Mod. Phys.* **82**, 1155 (2010).
- [46] D. F. Walls and G. J. Milburn, *Quantum Optics* (Springer, 2nd edition, 2008).

- [47] D. Witthaut and A. S. Sørensen, Photon scattering by a three-level emitter in a one-dimensional waveguide, *New J. Phys.* **12**, 043052 (2010).
- [48] S. Fan, Ş. E. Kocabaş, and J.-T. Shen, Input-output formalism for few-photon transport in one-dimensional nanophotonic waveguides coupled to a qubit, *Phys. Rev. A* **82**, 063821 (2010).
- [49] J. Dalibard, Y. Castin, and K. Mølmer, Wave-function approach to dissipative processes in quantum optics, *Phys. Rev. Lett.* **68**, 580 (1992).
- [50] C. Gardiner and M. Collett, Input and output in damped quantum systems: Quantum stochastic differential equations and the master equation, *Phys. Rev. A* **31**, 3761 (1985).
- [51] K. Mølmer, Y. Castin, and J. Dalibard, Monte Carlo wave-function method in quantum optics, *J. Opt. Soc. Am. B* **10**, 524 (1993).
- [52] C. R. Murray, A. V. Gorshkov, and T. Pohl, Many-body decoherence dynamics and optimized operation of a single-photon switch, *New J. Phys.* **18**, 092001 (2016).
- [53] A. V. Gorshkov, A. André, M. D. Lukin, and A. S. Sørensen, Photon storage in Λ -type optically dense atomic media. I. Cavity model, *Phys. Rev. A* **76**, 033804 (2007).
- [54] A. V. Gorshkov, A. André, M. D. Lukin, and A. S. Sørensen, Photon storage in Λ -type optically dense atomic media. II. Free-space model, *Phys. Rev. A* **76**, 033805 (2007).
- [55] E. Zeuthen, M. J. Gullans, M. F. Maghrebi, and A. Gorshkov, Correlated Photon Dynamics in Dissipative Rydberg Media, *Phys. Rev. Lett.* **117**, 043602 (2017).
- [56] D. Pinotsi and A. Imamoglu, Single Photon Absorption by a Single Quantum Emitter, *Phys. Rev. Lett.* **100**, 093603 (2008).
- [57] J. Vaneeccloo, S. Garcia and A. Ourjoumtsev, Intracavity Rydberg Superatom for Optical Quantum Engineering: Coherent Control, Single-Shot Detection, and Optical π Phase Shift, *Phys. Rev. X* **12**, 021034 (2022).
- [58] T. Stolz, H. Hegels, M. Winter, B. Röhr, Y. Hsiao, L. Husel, G. Rempe and S. Dürr, Quantum-Logic Gate between Two Optical Photons with an Average Efficiency above 40%, *Phys. Rev. X* **12**, 021035 (2022).